Dynamical Climatology

CO_2 climate sensitivity and model dependence of results.

by

J.F.B.Mitchell, C.A.Wilson and W.M.Cunnington

DCTN 28

September 1985

Meteorological Office (Met. O. 20)
London Road
Bracknell
Berkshire RG12 2SZ

DYNAMICAL CLIMATOLOGY TECHNICAL NOTE NO. 28

CO_2 CLIMATE SENSITIVITY AND MODEL DEPENDENCE OF RESULTS

by

J F B Mitchell, C A Wilson and W M Cunnington

Submitted for publication in Quart. J. Roy. Meteorol. Soc.

Met O 20 (Dynamical
Climatology Branch)
Meteorological Office
London Road
Bracknell
Berkshire, U.K. RG12 2SZ

September 1985

Note: This paper has not been published. Permission to quote from it should be obtained from the Assistant Director of the above Meteorological Office Branch.

Abstract

The regional response of climate models to small perturbations is shown to be highly dependent on the unperturbed simulation. An experiment in which CO_2 concentrations are doubled and sea surface temperatures are enhanced by 2°C has been carried out with two general circulation models which differ considerably in their control climates. The resulting changes in tropical precipitation in each model simulation are related to the increase in atmospheric water vapour which leads to enhanced precipitation in the main regions of low level atmospheric convergence. Since these regions of convergence occur in slightly different locations in the unperturbed simulations, the distribution of changes is also different.

Differences in control simulations must be taken into account when comparing results from different models (for example, on doubling atmospheric CO_2); otherwise unduly pessimistic conclusions may be reached concerning the consistency of model results. One may be able to make subjective allowance for the effect of known deficiencies in the unperturbed simulation on the model's response before using the simulated changes in, for example, impact studies.

A detailed examination of one of the experiments reveals that the change in precipitation is limited by the heat balance of the atmosphere. The magnitude of the model's response is shown to be consistent with that found in three-dimensional climate models which include a simple representation of the ocean.

1. Introduction

Over recent years, increasing use has been made of numerical models in climate research. Three dimensional general circulation models have been used extensively to study the atmospheric circulation, and, not surprisingly, it is found that the simulated climate varies with the model used. Attempts have been made to understand the reasons for differences in simulations (for example, GARP 1979), but the results are generally speculative because the models compared differ in more than one way. In principle, discrepancies between two models could be resolved by removing the differences one at a time (for example, Hansen et al 1983); in practice this would involve extensive co-operation between the institutions involved, and may be impossible, for example, where the physical processes of a particular model are interdependent. Thus, we are left with the unsatisfactory position in which model simulations differ from each other (and observed climate) for reasons which are not well understood.

Many climate models have been used to study the effect of increased atmospheric CO_2 concentrations on climate (Dickinson 1985, United States Department of Energy 1985). It is estimated that a doubling of atmospheric CO_2 concentrations would increase the net radiative heating below the tropopause by 4 Wm^{-2}, which is small compared to the 240 Wm^{-2} outward long wave flux at the top of the atmosphere. Thus a doubling or quadrupling of CO_2 amounts can be regarded as a perturbation on present day climate. This is confirmed by numerical studies where it has been found that changes in circulation are small (for example, Manabe et al 1981, Washington and Meehl 1984). It follows that the results of such sensitivity studies may be highly dependent on the simulation of the unperturbed climate, which in

turn depends on the model used. Given the wide variety of models used to date, it is not surprising that the results obtained are often contradictory.

The dependence of a model's sensitivity on its unperturbed climate should not be confused with dependence on the physical processes included in the model. For example, it is possible to construct two versions of a model, one with prescribed cloud, another with model-generated cloud, which would produce indistinguishable simulations of present day mean climate, but would respond quite differently to a given perturbation. Thus, an accurate representation of present day mean climate is not sufficient to guarantee that a model's sensitivity is correct. Here we are more concerned with the differences in sensitivity between models which include the same physical processes but produce different errors in the control simulation. For small perturbations, the simulated changes in climate will inevitably be strongly related to the control simulations. Since it will be some time (if ever) before present climate can be simulated without appreciable error, the likely effect of such errors on the simulated response to a given perturbation must be assessed.

Some progress towards this end has already been made. Hansen et al (1984) and Spelman and Manabe (1984) have demonstrated the dependence of the sensitivity of global mean surface temperature on the areal extent of sea ice, or sea ice and snow cover. A warming of the surface will remove some of the highly reflective snow or ice cover, producing further warming through enhanced absorption of solar radiation, often referred to as 'temperature-albedo feedback'. If the temperature in the control simulation is reduced, the latitude of the snow or ice boundary is reduced, the length of the boundary is increased and the mean solar elevation at the

boundary becomes higher. Temperature albedo feedback becomes stronger, and occurs over a larger area, and the sensitivity of the surface temperature is increased.

There is also evidence that the nature of the control simulation can affect changes on a continental scale. Several studies of the effect of increasing atmospheric CO_2 (for example, Manabe et al 1981, Mitchell and Lupton 1984) show a drying of the surface of the mid-latitude continents in the summer, despite the accumulation of extra soil moisture during winter. Much of this excess moisture gained in winter is lost as run-off in spring, when the model surface reaches field capacity over much of the area. A longer drying season and reduced precipitation then produce a drying of the surface in summer. In contrast, Washington and Meehl (1984) find ~~that~~ soil moisture increases throughout the year, ~~but~~ the increase is least pronounced in winter. In their model, the soil does not become saturated in spring, (~~Dickinson~~, private communication) so one may speculate that all the excess moisture accumulated in the winter must be lost over the summer by evaporation. The presence of enhanced soil moisture at the beginning of summer may lead to increased precipitation (Rowntree and Bolton, 1983, Yeh et al 1984). Indeed, Washington and Meehl find an increase in precipitation in northern mid-latitudes in summer, which further counteracts the tendency for enhanced evaporation to dry out the surface.

Little can be said about the smaller scale changes found in experiments with increased CO_2. Many simulations carried out to date have used low horizontal resolution and so cannot resolve regional detail. Furthermore, the comparison of the control and anomaly integrations has been limited to a few years, which may be insufficient to distinguish regional changes from the year to year variability on that scale. This is

unfortunate, since predictions on a regional scale are required before the potential social and economic impact of climate change due to increased CO_2 can be assessed.

Mitchell (1983), using a model with relatively high horizontal resolution, did find changes in regional precipitation which were statistically significant and physically reasonable. On increasing sea surface temperatures and doubling CO_2 amounts, significant changes in the precipitation were produced over the eastern sub-tropical continents in summer and in other regions. The consistency of these regional changes has encouraged us to repeat the experiment using a different model, in order to assess the model dependence of the results, and whether or not any discrepancies between the responses could be related to differences in simulations of the unperturbed climate.

In this paper it is not our intention to give a detailed explanation of the differences in the control simulations in terms of the model formulations.

Here, we

(1) Describe the changes found on doubling CO_2 and increasing sea surface temperatures by 2K in a version of the Meteorological Office 11 layer general circulation model (11 LM).

(2) Compare the results with those in a similar experiment using the Meteorological Office 5 layer general circulation model (5 LM, Mitchell 1983).

(3) Relate differences in response of the two models to differences in the control simulations, where appropriate.

(4) Identify the physical mechanisms common to both experiments and discuss the implications of the above work for numerical studies of climate change.

2. The Models

The 11-layer model is the original global version of the 11 layer limited area tropical model developed for the GARP Atlantic Tropical Experiment (Lyne et al, 1976). The 11 sigma (σ = pressure/surface pressure) layers are irregularly spaced, being concentrated near the boundary layer and the tropopause. A 2.5° x 3.75° latitude/longitude horizontal grid has been used. The seasonal and diurnal variation of solar radiation are represented, and the radiative fluxes are a function of temperature, water vapour, carbon dioxide and ozone concentration, and prescribed zonally averaged cloudiness. Long wave fluxes are calculated using the emissivity approximation. Sea surface temperatures and sea ice extents are prescribed from climatology, and updated every 5 days. The heat flux through sea ice is included.

The treatment of the boundary layer, which occupies the lowest 3 model layers, is based on Method I of Clarke (1970). The calculation of fluxes of heat, moisture and momentum from the surface is based on Monin-Obukhov similarity theory. Evaporation is limited, where appropriate, by soil moisture following Manabe (1969). Convection is modelled using a penetrative scheme in which both entrainment of environmental air and detrainment from the convective parcel are allowed at each level. Excess moisture due to condensation following convection or large scale ascent is removed as precipitation.

The 5-layer model uses a similar finite difference scheme on a quasi uniform 330 km horizontal grid, with five equally spaced sigma layers in the vertical (Corby et al 1977). The treatment of radiation, sea surface temperatures, sea ice extents, cloud amounts, and soil moisture, described by Slingo (1982), is similar to that in the 11-layer model. The penetrative convection scheme is less intricate than that used in the 11 layer model. The boundary layer height is modelled explicitly, and used to control surface fluxes and, where appropriate, convection.

The main differences in the formulation of the two models are listed in Table 1. A comparison of a version of the 11 layer model on a 220 km quasi-uniform grid with the 5 LM was made by Mitchell and Bolton (1983). The 11 layer model produced a superior simulation of the general circulation with greater transient activity and a more realistic simulation of the mid latitude depression tracks, except in the northern hemisphere in winter. The 5 layer model tends to produce too much precipitation over land, whereas in the 11 layer model it is excessive over the tropical oceans.

The control integration in the 11 layer model experiment was run for 8 years starting from real initial data from the First GARP Global Experiment (July 25th 1979). The anomaly integration was started from 1st March of the second year of the control, and run for 3 years. Seasonal differences calculated from averages of the 8 years of the control and the 3 years of the anomaly simulation are presented; annual mean quantities are computed from the period corresponding to the last 2 years of the anomaly integration. The 5-layer model control integration was run for 3 years and the anomaly for $2^1/_2$ years (Mitchell, 1983). Differences are computed over the final two years of the anomaly integration.

3. The models' responses

a. Global annual mean

The globally averaged response of the 11 layer model is similar to that of the 5-layer model (Table 2). The increase in sea surface temperature raises the saturation vapour pressure at the ocean surface and evaporation increases by 5.6% (6.6% in the 5-layer model). The total atmospheric moisture content increases by 20% (18%) and precipitation by 5.6% (4.9%). The troposphere warms by 3.1 (3.0)°C, largely due to the increased release of latent heat, and the land surface warms by 3.1 (2.9)°C as a result of the increased downward flux of infrared radiation from the warmer, moister CO_2-enriched atmosphere. In the evaluation of climatic impacts, the regional supply of moisture to the surface (precipitation minus evaporation, or P-E) is of more interest than the global mean change in precipitation. The mean magnitude of P-E increases from 1.15 (1.72) mm/day by 0.15 (0.17) mm/day or 13 (10)%, substantially more than the percentage change in global mean precipitation.

b. Spatial and Temporal Variations

i. Temperature, humidity and zonal wind. The top of the model cools, following increased radiation loss to space from the enhanced CO_2 (Figure 1). The troposphere warms, due to the enhanced release of latent heat. The model's moist convective processes tend to adjust the vertical profile towards the moist adiabatic lapse rate, which becomes smaller with increasing temperature, so that temperature changes are amplified with height. The 5°C increase at 300 mb in the tropics is consistent with increasing the surface temperature by 2°C and maintaining a

moist adiabatic temperature profile. Note that in studies carried out with models employing a moist convective adjustment scheme (for example, Manabe and Stouffer, 1980; Washington and Meehl, 1984) the amplification of the temperature increase with height is much less pronounced than in studies where a penetrative convection scheme has been used as here and in Hansen et al (1984).

In a moist convective adjustment scheme, adjacent pairs of layers are considered in succession for instability (or potential instability). If the profile between two layers is unstable, the air in two layers is mixed until the instability is removed. Thus, if the scheme is presented with a saturated unstable profile, illustrated schematically in figure 2, it will produce a uniform profile of wet bulb potential temperature extending to a. In a penetrative scheme, air from a given level can rise to the limit given by convective parcel theory. In principle, air parcels adjacent to the surface in our example can penetrate to b, though in practice, this limit would not be reached as most penetrative schemes allow for entrainment of environmental air which reduces the buoyancy of convective parcels. Even so, the penetrative scheme will warm to a higher level and (because both schemes conserve moist static energy) produce a slightly cooler profile at lower levels. In summary, the penetrative scheme will produce a larger response at upper levels to a given surface warming as it moves heat and moisture to higher levels than the convective adjustment scheme.

The height and magnitude of the maximum warming decrease towards the poles, increasing the meridional temperature gradient in the upper troposphere, particularly near 40° of latitude. In the sub-tropics (near 25° of latitude in winter and 35° in summer), a tongue of warmer air extends downwards from the upper troposphere, reducing the meridional temperature gradient at mid-levels in the tropics. One may speculate that air near the top of the ascending branch of the equatorial Hadley circulation where the warming is largest, is carried poleward and subsides in the sub-tropics, further warming the middle troposphere. Since the descending branch of the Hadley circulation in the summer hemisphere is about five times weaker than in the winter hemisphere, the symmetry of the changes indicates that other mechanisms such as longitudinal circulation may contribute to the warming at mid-levels in the sub-tropics. In middle latitudes, the tropospheric warming is a minimum, although the reasons for this are not clear. There is a secondary maximum warming in high latitudes which, in the winter hemisphere, varies considerably from year to year.

Zonally averaged relative humidity calculated from seasonal means of temperature, humidity and pressure (Figure 3) is reduced in the upper troposphere, with maximum reductions of over 10% in the equatorial region. The main increases occur in the lower stratosphere except in the subtropics and in the tropics in the middle troposphere; small increases are found in the lower troposphere at most latitudes.

The changes in zonally averaged west to east wind (Figure 4) are largely those expected assuming geostrophic balance with the changes in geopotential gradients implied by the temperature changes in Figure 1. For example, near 40° of latitude, there is enhanced westerly flow particularly at upper levels associated with the increased meridional temperature gradient, whereas further poleward, where this gradient is decreased, the westerly flow is weakened. Outside the tropics, the sign of the changes in zonal wind is constant with height, probably due to mixing of momentum in the vertical by large scale motions. The increased flow at near 75°N in December to February (Figure 4b) and near 50°S in June to August is associated with a tendency for the winter surface pressure trough to be deeper in the anomaly integration.

The changes in temperature in the 5 layer model were remarkably similar (Figure 5), except in the upper troposphere near 40° of latitude in summer, where a spurious warming occurs due to a deficiency in interpolation of the humidity profile for use in calculating the radiative fluxes (see Mitchell, 1983). As a result of this error, the associated increase in meridional gradient is further poleward than in the 11 layer model, and the enhanced westerly flow in summer is found poleward of the maximum in the control (Figure 6) rather than equatorward as in the 11 layer model.

The zonally averaged surface pressure trough is found near 60°N and 60°S in local winter in the 5 layer model, and further poleward at 70°N and 65°S in the 11 layer model. In both models,

the winter depression belts and associated westerlies intensify, with the enhanced westerly flow occurring further poleward in the 11 LM. However, in the 11 LM in the northern hemisphere in winter, (Fig 4b) the enhancement increases with height, and there is a further region of increased flow at upper levels near 30°N. In the 5 LM, (Figure 6b), there is a single band of enhanced westerly flow near 65°N in winter which falls off with height. This discrepancy between the responses in the two models is due in part to an erroneous low level maximum in westerly flow near 55°N in the 11 LM.

In summary, the zonally averaged response of the models is similar in many respects, and most of the discrepancies that do occur can be explained directly in terms of the differences in model formulation, or related to differences in the unperturbed simulation.

ii. Precipitation

As noted earlier, the moisture content of the atmosphere increases in the anomaly integration. Mitchell (1983) argued that in the absence of changes in circulation, this should lead to an increase in precipitation (or more accurately, precipitation minus evaporation) in regions of low level mass convergence due to increased moisture convergence, and conversely a decrease in precipitation in regions of low level mass divergence. If one assumes that storage in the atmosphere and diffusion of moisture can be ignored, the equation for moisture (see Corby et al 1977) can be integrated in the vertical to give

$$\frac{1}{p*} \int \underline{\nabla} \cdot (\underline{V} \; P* \; q) \, d\sigma = E-P \qquad (1)$$

where P_* is surface pressure, V is the velocity on σ levels, q is the specific humidity and σ is the vertical coordinate.

Mitchell's hypothesis then follows, noting that the main contribution to the vertical integral comes from the lower troposphere, and assuming that the fractional change in specific humidity in the lower troposphere is fairly uniform. In the 11 LM, zonally averaged precipitation increases in the main regions of convergence in the equatorial pressure trough and in middle to high latitudes (Figure 7). The enhancement in precipitation in winter mid-latitudes is further increased by stronger low-level mass convergence accompanying the deepening of the depression tracks noted above. In the sub-tropics, precipitation changes little although evaporation increases markedly, so precipitation minus evaporation and hence moisture convergence are reduced.

In general, the peaks in precipitation become more intense (for example at 60°N, 10°S, 50°S in December to February (Figure 7b), though the mid-latitude peak shifts poleward in winter (from 35°N in December to February and 40°S in June to August). The broad pattern of the response is similar in the 5 layer model experiment (enhancement of the equatorial and mid-latitude peaks, poleward shift of the winter mid-latitude peak and little change in the sub-tropics (Figure 8)), though the distribution of the changes differs in detail. This to a large extent reflects the differences in the two control simulations; for example, in the 11 layer model the simulated precipitation shows two peaks in the equatorial regions (Figure 7),

associated with more than one zone of increase, whereas in the 5 layer model both the equatorial peak in precipitation and associated regions of increase are more coherent (Figure 8).

The most intense changes occur in the tropics (Figure 9), with large increases in regions of strong low level convergence. In the sub-tropics and middle latitudes, the response is less pronounced, though over land precipitation is generally reduced, especially during June to August (Figure 9a). Precipitation is enhanced in high latitudes, particularly in winter.

In the tropics the detailed changes are not random, being closely related to the unperturbed pattern. (The statistical significance of the changes in precipitation are discussed in the Appendix). Regions of increase generally coincide with areas where precipitation is already intense in the control simulation, as one would expect if the changes are dominated by the increase in atmospheric moisture as opposed to changes in circulation. Thus in the northern hemisphere north of the equator during June to August, rainfall is enhanced over the central Pacific and western Atlantic oceans, off the south eastern United States, in the Bay of Bengal and to the east and west of the Phillipines (Figure 9a), corresponding to maxima in the control integrations (Figure 10). Increases occur south of the equator in the Indian and Central Pacific Oceans where there is strong low level convergence in the control integration.

This pattern is repeated in December to February (Figure 9b) north of the equator over the tropical east Pacific Ocean and east of the Phillipines, and south of the Equator in the Central Pacific and western Indian Oceans, east of South America and Australia and over

Indonesia, but not north of the equator over the west Atlantic and Indian Oceans, and over Indonesia and South America near 20°S where rainfall is decreased over wet regions.

In mid latitudes the relationship between the control simulation and the response is less obvious. For example, in December to February (Figure 9b) precipitation is enhanced over southern Alaska and west of Scandinavia as expected, but also in the north Atlantic well to the east of the rainband off eastern north America. Precipitation decreases in many regions where it is already meagre, for example over the south west of North America and from the Mediterranean eastwards in June to August. Over land, changes in E-P may be limited by the availability of soil moisture. In regions of prevailing moisture divergence (for example, over much of the mid-latitude continents in summer) an increase in moisture divergence and E-P will enhance the drying of the surface, and may ultimately produce a reduction in both evaporation and precipitation.

A similar correlation between the patterns of precipitation in the unperturbed simulation and patterns in the response is evident in the 5 layer model (Figures 11, 12). It can also be seen that in the 5 layer model, the heaviest precipitation occurs over land (around the Caribbean, over east Africa and the Indonesian islands, along the southern and eastern coasts of North America and Asia in June to August, (Figure 12a) and over northern and eastern south America, east Africa and the Indonesian islands during December to February, (Figure 12b), whereas in the 11 layer model, the heaviest precipitation is found in the same general regions,but occurs predominantly over the ocean (Figure 10). Although in both models,

the increase in atmospheric moisture appears to be the dominant mechanism producing the changes in precipitation the distribution of the response is different because the unperturbed simulations are different. Thus, in the 5 layer model, there is a much larger response over land than in the 11 layer model (Table 3). This is reflected in the geographical distribution of the response, as around the southern coasts of the Caribbean and south east Asia during June to August (Figure 9a, 11a). In short, the pattern of the model's response is strongly dependent on the unperturbed simulation.

In order to quantify the relationship between the model's response and the unperturbed simulation, we have calculated the spatial correlation between P-E and changes in P-E (see Appendix). If the atmospheric circulation is unchanged and the fractional change in humidity is uniform, the correlation coefficient should be unity (see equation 1). The spatial correlation is 0.36 (0.28 in the 5 LM) for the annual mean if the whole globe is considered. The correlation is 0.39 if only the tropical oceans (30°N to 30°N) are considered, and is considerably higher in the extra tropics (poleward of 30°, see Appendix). Our estimate of the correlation coefficient is biased downwards due to the temporal variability of the model. If a simple correction is made to allow for this (see Appendix), the above figures are increased to, 0.59 (0.35 in the 5 LM) and 0.63 respectively. Thus for example, our hypothesis accounts for approximately 40% of the spatial variance in the changes in P-E over the tropical oceans if the contribution from temporal variations is removed.

4. Discussion

a. Assessment of the model's response

The similarity of the global mean response in the two models indicates that the magnitude of the simulated changes is governed by the same factors. In this subsection we consider the nature of the simulated response and compare it with that expected on the basis of certain simple assumptions.

i. Temperature and humidity

The surface temperature is increased by 2°C over the two thirds of the earth's surface which is ocean where moisture is unlimited. The lapse rate over much of the oceans, particularly in the tropics, is close to moist adiabatic; the vertical profile of temperature changes is largely consistent with increasing the surface temperature by 2°C and maintaining a moist adiabatic temperature profile (Figures 1 and 5, section 3b).

The changes in globally averaged humidity at each level in the 11 LM (Table 4) are broadly consistent with the assumption that relative humidity remains constant. The percentage increase in humidity mixing ratio reaches a maximum in the upper troposphere where temperature increases are largest. Note also that the fractional change in saturation vapour pressure for a given change in temperature is larger at lower temperatures (changes in relative humidity were discussed in section 3b).

ii. Precipitation and the atmospheric heat balance

Increasing the surface temperature from 15°C (the global mean) by 2°C increases the saturation vapour pressure at the surface by 13%. In the absence of marked changes in the static stability, wind speed and relative humidity of the bottom layer, evaporation and hence precipitation would increase by approximately the same amount. The simulated increase in precipitation is only 5.6%(4.9% in the 5 LM), or about half that expected on the basis of the above assumptions. Kandel (1981) examined the surface energy budgets reported in several studies on the effect of increased atmospheric CO_2 and concluded that the sensitivity of surface temperature (when free to respond to the change in CO_2) depended critically on the constraints on evaporation and atmospheric humidity. In the present work, the change in surface temperature over the oceans is prescribed and is therefore independent of the surface energy budget. However, the changes in latent heat release to the atmosphere must balance other changes in the atmospheric heat budget. This we now consider in detail to identify the factors which influence changes in latent heat release, and hence precipitation in the 11 LM experiment.

The 5 Wm^{-2} increase in latent heat release (Table 5) is balanced by a small decrease in the flux of sensible heat, and a 4 Wm^{-2} increase in radiative cooling. The latter comprises a 2.6 Wm^{-2} warming due to the increased absorption of solar radiation, and a cooling of 6.8 Wm^{-2} due to the enhanced divergence of

longwave radiation (note that here we are considering the heat balance of the atmosphere in isolation, not the atmosphere and surface).

The contribution of the increases in CO_2, water vapour and temperature to the enhanced long wave cooling have been estimated by taking the annual mean profile at each grid point, running the radiation code with the changes applied one at a time, and globally averaging the results, (Table 6). The effect of applying all three changes simultaneously was also estimated, and found to be in close agreement with that found in the integration of the full model shown in Table 6 (last column).

Doubling CO_2 amounts reduced the outgoing longwave flux at the top of the atmosphere by 2.1 Wm^{-2}. The increase in the downward flux at the surface is smaller, as the lower atmosphere is optically thicker at the wavelengths at which CO_2 is active. Enhanced downward radiation from upper levels is thus absorbed, and not 'seen' by the surface. As a result, increasing CO_2 amounts produce a direct warming of the atmosphere. In contrast, the change in downward flux at the surface due to enhanced water vapour is greater than that at the top of the model because the upper atmosphere is optically thin over much of the spectrum where water vapour absorbs radiation. As a consequence, enhancing water vapour produces a slight cooling of the atmosphere at infrared wavelengths. The increase in surface and atmospheric temperatures produces a net cooling of over 6 Wm^{-2}, largely due to increased cooling to space.

We further assume, on the basis of single column experiments, that about 1 Wm^{-2} of the 2.6 Wm^{-2} increase in solar absorption is due to doubling CO_2 and the remaining 1.6 Wm^{-2} is due to increases in water vapour. Thus doubling CO_2 reduces the atmospheric radiative cooling by about 2 Wm^{-2}; water vapour has little effect on atmospheric heating rates, since the enhanced longwave cooling is largely compensated by solar heating, whereas the temperature increases enhance radiative cooling by about 6 Wm^{-2} (Table 6).

As noted earlier, the 4 Wm^{-2} net increase in radiative cooling is balanced by increased latent heat release (and a small reduction in sensible heating). The 13% increase in evaporation and precipitation deduced from the simple assumptions outlined at the beginning of the subsection would produce an increase in latent heat release of 12 Wm^{-2}. It would require a substantial alteration in the vertical distribution of the changes in temperature and humidity to increase the 4 Wm^{-2} to the 12 Wm^{-2} postulated above. For example further temperature increases in the boundary layer would increase the static stability at the surface reducing evaporation; increases at upper levels would increase the static stability of the troposphere and suppress convective instability. Similarly, further increases in boundary layer humidities would reduce evaporation. Further increases in moisture at upper levels would be limited by saturation, and would not contribute greatly to the net radiative cooling of the atmosphere. Thus it seems that constraints on changes in static stability and radiative cooling reduce the changes in evaporation

and precipitation below that expected on the basis of constant relative humidity. Note that the simulated increase in relative humidity at lower levels (Figure 3) is consistent with reduction of the change in evaporation below the 'expected' 13%; the decrease in relative humidity at upper levels is consistent with a similar shortfall in precipitation.

iii. Precipitation minus Evaporation (P-E).

From equation (1), if it is assumed that changes in circulation (represented by V) are small and that the fractional increase in humidity is uniformly distributed, then the changes in $|E-P|$ will be proportional to changes in q, and the 20% rise in humidity should be accompanied by a similar increase in the magnitude of P-E. However $|P-E|$ increases by considerably less (13%), as the fractional increase in specific humidity is not distributed uniformly, but increases with height (Table 4) and the largest contribution to the vertical integral in (1) comes from the lower troposphere, since humidity decreases rapidly with height, and the mass convergence in the middle troposphere is small. Even so, the fractional change in $|P-E|$ is smaller than the change in humidity in the boundary layer, indicating that changes in circulation, or horizontal variations in the fractional change in humidity also contribute to changes in P-E.

b. Effects of increased CO_2

Mitchell (1983) discussed the relevance of the 5 layer model experiment to the problems of increased CO_2 and climate. Here, we follow his approach, assuming that the response of the model to small changes in sea surface temperature is linear, and that the effects of CO_2 and sea surface temperature are additive. Mitchell found an increase of 3.5 Wm^{-2} in net surface heating due to doubling CO_2 amounts alone. Surface heating is reduced by 1.2 Wm^{-2} due to doubling CO_2 and increasing sea temperatures by 2°C in the 11 LM. A 2°C increase in sea surface temperatures alone might therefore be expected to reduce the net surface heating by 4.7 ie (3.5 + 1.2) Wm^{-2}. For the changes in CO_2 and sea surface temperatures to be in balance, the change in net surface heating should be zero, and would require a sea surface temperature increase of 1.5 (ie 2 x 3.5/4.7)°C, or a reduction of 25% from the present experiment, to balance the 3.5 Wm^{-2} increase in surface heating due to doubling CO_2. The corresponding changes in global mean surface temperature (allowing for land) and precipitation would be 1.72°C and 4.2% respectively, in broad agreement with the 2.0°C and 3.4% obtained by Manabe and Stouffer (1980) using an atmospheric model coupled to a rudimentary model of the upper ocean (if one assumes that a quadrupling of CO_2 amounts has twice the effect of doubling).

In view of the relationship between precipitation and the atmospheric heat balance discussed in section 4.a.ii, a better estimate of the precipitation change at equilibrium can be given. Assuming the tropospheric temperature change, and hence the

associated changes in sensible heat and net long wave cooling of the atmosphere are also reduced by 25%, the resultant cooling of the atmosphere due to changes in temperature alone would be 0.75 x (6.3 + 0.7) = 5.25 Wm^{-2} (see Table 6). This must be balanced by contributions due to changes in water vapour (negligible), CO_2 (1.9 Wm^{-2}) and precipitation. This implies an enhancement of latent heat release of 3.35 Wm^{-2}, corresponding to a 3.8% increase in precipitation.

The surface warming is smaller than in other studies of the effect of doubling CO_2 amounts (Hansen et al, 1984; Washington and Meehl, 1984; Manabe, 1984, personal communication). In those studies the response to increased CO_2 was amplified by reductions in sea-ice extents and changes in cloud cover; here the distributions of cloud and sea-ice were prescribed and unchanged.

5. Summary and concluding remarks

The responses of two general circulation models to doubling CO_2 concentrations and prescribing a 2°C increase in sea surface temperatures have been compared. The main findings are:

1. The large scale response is similar in both models. The following features were identified as being common to both experiments.

   a. The models produce a vertical profile of temperature changes consistent with maintaining a moist adiabatic lapse rate, giving temperature increases which increase with height from about 2°C near the surface up to 5°C in the tropical upper troposphere.

b. To a first approximation, the atmospheric moisture content increases so that relative humidity is unchanged. The main deviations from this generalisation occur in the upper troposphere, where relative humidity is reduced, and in the lower stratosphere and near the surface, where it is increased.

c. Precipitation is increased where it is already heavy due to the increase in specific humidity leading directly to increased moisture convergence. Conversely precipitation changes little or decreases where it is meagre in the control simulation.

d. The magnitude of the changes in the supply of moisture to the ground (P-E) is roughly proportional to the change in atmospheric moisture content in the lower atmosphere, which in turn is related to the change in atmospheric temperature through the Clausius-Clapeyron relation. The change in global mean precipitation is smaller, being limited by the atmospheric heat balance.

2. On a regional scale, although there is some agreement, important differences do occur, as shown for precipitation. Many of these discrepancies can be related to differences in the control simulation. This is to be expected since the changes in the model boundary conditions are small enough to be regarded as a perturbation.

3. In comparing the results from different models used to investigate the effect of perturbations on climate, for example due to increased atmospheric CO_2, one needs to assess the influence of the different model formulations. This may be extremely difficult because the models are likely to differ in more than one respect. Alternatively, one can identify the physical mechanisms which dominate

the simulated response in each model. If the same mechanisms operate, one can then assess the likely effect of differences in unperturbed simulations on each model's response. Failure to do so will lead to unnecessarily pessimistic conclusions concerning the consistency of numerical studies of climate and climate change.

4. The close relationship between unperturbed climate and climate change indicates that it is necessary (though not sufficient) to use a model which simulates the present day climate accurately if it is to produce accurate estimates of climate change. It may be possible to allow for some of the discrepancies between observed and simulated climate provided the physical mechanisms which dominate the modelled response have been identified (and are realistic). This is analogous to the interpretation of forecasts from early numerical prediction models, allowance being made for known biases in the model.

6. Acknowledgements. We thank Andrew Gilchrist, Peter Rowntree and Howard Cattle for useful comments and discussions. This work was supported in part by E.E.C. Contract no. CLI - 030 - 81 - UK(H).

Appendix (a) Statistical Significance of Results

Simulations made with a general circulation model exhibit apparently random year to year fluctuations which are a manifestation of the model's inherent natural variability. In order to distinguish those differences between the anomaly and control simulations which are unlikely to have occurred by chance, and are therefore probably due to the enhancement of sea surface temperatures and CO_2 amounts, we have performed a simple significance test.

A 2-tailed Student's t-test was carried out using seasonal means (3 from the anomaly, 8 from the control) of precipitation in the 11 LM experiment (Figure 11). Results of a similar test on the 5 LM results were reported by Mitchell (1983). Here, there are systematic patterns of change significant at the 90% level of confidence or higher in high latitudes in December to February, and in the tropics during June to August. The patterns are less well organised in the tropics during December to January, although the increases in regions of existing heavy precipitation are generally significant.

The limitations of the above test must be borne in mind. First, as meteorological patterns are correlated in space, coherent areas of apparently significant changes will occur by chance. Hannoschock and Frankignoul (1984) have tried an approach proposed by Hasselmann (1979) using a reduced basis set which may overcome this shortcoming, but is unsuitable for use with fields such as precipitation which vary on a small spatial scale. Second, for random samples from the same population, a certain fraction of points (on <u>average</u> A) will appear significant at the (1-A) level of confidence. One can test if the field from the anomaly

experiment is significantly different from the field in the control (Preisendorfer and Barnett, 1983, Livezey and Chen, 1983), but such tests do not indicate where the fields are significantly different. Third, since the distribution of precipitation deviates from the normal distribution (Reed 1985) assumed in the test, the significance levels should be regarded as relative rather than absolute. Most emphasis should be placed on those aspects of the model's response which have been explained on a physical basis.

From Table A1, it can be seen that the percentage area with precipitation changes significant at the 90% level of confidence is consistently higher than 20% throughout the year. According to Livezey and Chen (1983, Figure 6) this change in the field of precipitation is significant at the 90% level of confidence provided the number of spatial degrees of freedom is greater than 25. There is no generally accepted method for establishing the number of degrees of freedom, but given the small spatial scales on which precipitation varies in the model, it is exceedingly unlikely that it is less than 25. Also given in Table A1 are the percentage areas with precipitation changes significant at the 90% level, when two sets of three years data (four for Spring) from the control integration are compared. The average value 9.7% is close to the expected value (10%) for a large number of tests from a population of normally distributed variables.

(b) Estimates of the spatial correlation coefficient

The spatial correlation coefficient $\rho_{p,q}$ between fields p and q is defined by

$$\rho_{p,q} = \frac{\text{covar } (p,q)}{\sqrt{\text{var } (p) \times \text{var } (q)}}$$

where, for example, the spatial variance var (p) is given by $(p_i - P)^2$. p_i is the value of p at position i, $P = \overline{p_i}$, and $\overline{\ }$ denotes the area weighted mean over the region of interest. In practice, the grid point values p_i and q_i fluctuate in time due to the model's inherent variability, and so must be estimated from the available samples. With N independent samples p_{ij} (j=1,N), the most obvious estimate of ρ_{pq} is obtained by replacing p_i by the temporal average $\frac{1}{N}\sum_{j=1}^{N} p_{ij}$, and so on. However, the temporal variability tends to inflate the temporal estimate of the spatial variance. For example, if the temporal variances of p_i and P are σ_i^2 and Δ^2 respectively, the expected value of the spatial variance of p estimated from a sample of size N, E (var (p)) is given by

$$\text{var}\ (p) + \frac{1}{N}\ (\sigma^2 - \Delta^2) \qquad \text{A2}$$

where $\sigma^2 = \overline{\sigma_i^2}$. Now $\sigma^2 - \Delta^2 \geq 0$, and in practice, $\sigma^2 >> \Delta^2$, so the expected value of the variance exceeds the actual value, especially for small samples. It can also be shown that

E (covar (p,q)) = covar (p,q)

provided temporal variations of p and q are not correlated in time.

We can estimate σ_i^2 and Δ^2 from the samples p_{ij} in the normal manner by s_i^2 and d^2 respectively, where

$$s_i^2 = \frac{1}{N-1}\sum_j (p_{ij} - \frac{1}{N}\sum_j p_{ij})^2$$
$$d^2 = \frac{1}{N-1}\sum_j (P_j - \frac{1}{N}\Sigma_j P_j)^2 \qquad \text{A3}$$

An unbiased estimate for var (p) is the sample variance reduced by $\frac{1}{N}(\sigma^2 - \Delta^2)$ which can then be used in (A1).

The correlation of p with q-p is given by

$$\rho_{p,q-p} = \frac{\text{Covar } (p,q) - \text{var } (p)}{\sqrt{\text{var } (p) \left[\text{var } (p) + \text{var } (q) - 2 \text{ covar } (p,q)\right]}}$$

Here p and q represent P-E sampled from the control and anomaly integration respectively, $\rho_{p,q-p}$ represents the correlation of changes in P-E with P-E. The global spatial correlations and corrected values are given in Table A2. It has been assumed that σ_i^2 and Δ^2 are the same in both the anomaly and control integrations, and σ_i^2 and Δ^2 were derived from the 8 year control integration from the 11 LM, and from the 3 year control integration of the 5 LM.

References

Clarke, R H 1970 Recommended methods for the treatment of the boundary layer in numerical models. Australian Met. Mag. 18, 51-73.

Corby, G A, Gilchrist, A and Rowntree, P R 1977 United Kingdom Meteorological Office Five Level General Circulation Model. Methods in Computational Physics, Vol 17, Academic Press Inc., New York, San Francisco and London, 67-110.

Dickinson, R E 1985 'Modelling of Future Climate'. In 'The climate response to an increased concentration of CO_2 and the Early Detection of CO_2 effects on climate'. WMO/ICSU/UNEP report prepared by IMI, Stockholm.

GARP 1979 Report of the JOC Conference on Climate Models; Performance, intercomparison and sensitivity studies. GARP Publication Series No. 22. ICSU/WMO.

Hannoschock, G and Frankignoul, C 1984 Multivariate Statistical Analysis of a sea surface temperature anomaly experiment with the GISS General Circulation Model. Submitted to JAS.

Hansen, J, Lacis, A, Rind, D, Russell, G, Stone, P, Fung, I, Ruedy, R and Lerner, J 1984 Climate Sensitivity; Analysis of Feedback Mechanisms in 'Climate Processes and Climate Sensitivity'. (Maurice Ewing Series, 5, eds J E Hansen and T Takahashi). A. G. U. Geophysical Monograph 29, Washington 368 pp.

Hansen, J, Russell, G, Stone, P, Lacis, A, Lebedeff, S, Ruedy, R and Travis, L 1983 Efficient three dimensional models for Climate Studies. Models I and II. Month. Weath. Rev. 111, 609-662.

Hasselmann, K 1979 'On the signal-to-noise problem in atmospheric response studies'. In 'Meteorology of the Tropical Oceans', D B Shaw ed., Roy. Meteor. Soc. 251-259.

Kandel R S 1981 Surface temperature sensitivity to increased atmospheric Co_2. Nature 293, 634-636.

Livezey, R E and Chen, W Y 1983 Statistical field significance and its determination by Monte Carlo techniques. Mon. Weather. Rev., 111, 46-59.

Lyne, W H, Rowntree,P R Temperton, C and Walker, Julia 1976 Numerical Modelling using GATE data. Met. Mag. 105, 261-271.

Manabe, S	1969	Climate and the ocean circulation I. The atmospheric circulation and the hydrology of the earth's surface. Month. Weath. Rev., 97, 739-774.
Manabe, S and Stouffer, R J	1980	Sensitivity of a Global Climate Model to an increase of CO_2 concentration in the atmosphere. J Geophysical Research 85, 5529-5554.
Manabe, S, Wetherald, R T and Stouffer, R T	1981	Summer dryness due to an increase of atmospheric CO_2 concentration. Climatic Change 3, 347-385.
Mitchell, J F B	1983	The seasonal response of a general circulation model to changes in CO_2 and sea surface temperature. Q.J.R. Met. Soc. 109, 113-152.
Mitchell, J F B and Bolton, J A	1983	Some differences between the Met O 20 5 and 11 layer models annual cycle integrations. Proceedings of ECMWF Workshop on Intercomparison of Large-scale Models used for extended range forecasts. (30 June-2 July 1982) 193-224.

Mitchell, J F B and Lupton, G — 1984 — A 4 x CO_2 experiment with prescribed in sea temperatures. Progress in Biometeorology. 3, 353-374. Paper presented at C.E.C. Symposium 'Interactions between climate and biosphere', Leith, Fantechi and Schnitzler, eds., Osnabruck, March 21-23, 1983.

Preisendorfer, R W and Barnett, T P — 1983 — 'Numerical Model-Reality Intercomparison Tests using small-sample statistics'. JAS. 40, 1884-1896.

Reed, D N — 1985 — Simulation of time series of temperature and precipitation over Eastern England. (Submitted to Journal of Climatology).

Rowntree, P R and Bolton, J A — 1983 — Simulation of the atmospheric response to soil moisture anomalies over Europe. Quart. J.R. Met. Soc. 109, 501-526.

Slingo, J M — 1982 — A study of the earth's radiation budget using a general circulation model. Q.J.R. Meteorol. Soc., 108, 379-405.

Spelman, M J and Manabe, S — 1984 — Influence of Oceanic Heat Transport Upon the Sensitivity of a Model Climate. J. Geophys. Res. 89, 571-586.

United States Department of Energy — 1985 — State of the Art Report on 'Climatic Effects of increasing CO_2 Concentrations' US Department of Energy, Washington DC. (In preparation).

Washington, W M and Meehl, G A 1984 Seasonal cycle experiment on the Climate Sensitivity Due to a Doubling of CO_2 with an Atmospheric General circulation Model Coupled to a Simple Mixed Layer Ocean Model. J. Geophys. Res., 89, 9475-9503.

Yeh, T C, Wetherald, R T and Manabe, S 1984 The Effect of Soil Moisture on the Short-Term Climate and Hydrology Change - A Numerical Experiment. Month. Weath. Rev. 112, 474-490.

Table 1 Main differences in model formulations

5 LAYER MODEL	11 LAYER MODEL
GRID 5 layers, equally spaced	11 layers, concentrated near surface and tropopause
300 km in horizontal	2.5° x 3.75°
BOUNDARY LAYER	
1 layer (up to $\sigma = 0.8$)	3 layers (up to $\sigma = .79$)
Explicit boundary layer height	Vertical diffusion, "Clarke" scheme
Bulk aerodynamic formula	Drag coefficient continuous
Stable/Unstable, land/sea drag coefficient	function of stability and roughness length
Full evap. when soil moisture = 10 cm	Full Evaporation ≃ 5 cm
Run off when soil moisture = 20 cm	Run off ≃ 15 cm
RADIATION	
Temperature and humidity interpolated to 10 equally spaced layers for radiation.	Fluxes calculated on model layer boundaries
No absorption of reflected solar beam.	Reflected solar beam absorbed
Snowfree albedo a function of latitude	Constant (= .2)
Albedo over snow a function of snow depth	Constant (= .5)
Cloud amounts, albedos similar	
PENETRATIVE CONVECTION	
Detrains only at upper levels	May entrain and detrain at any level.
May affect a given layer more than once/timestep.	Only affects a given layer once/timestep.
DIFFUSION	
Non-linear Diffusion of potential temperature θ	Non-linear Diffusion of $aT + b\theta$
Non linear diffusion of humidity	Linear diffusion of humidity.

Table 2 Changes due to doubling CO_2 and enhancing sea surface temperatures (Global 2 year mean)

	Tropospheric Temperature (°C)	Atmospheric Moisture Content (%)	Land Surface Temperature (°C)	Precipitation (%)
11 LM	3.08	20	3.05	5.6
5 LM	3.02	18	2.86	4.9

Table 3 Global annual mean precipitation in the 11 LM and 5 LM models, and changes due to doubling CO_2 and enhancing sea surface temperatures (mm/day).

	Precipitation			Changes		
	Globe	Land	Sea	Globe	Land	Sea
11 LM	3.02	2.00	3.44	0.17	0.03	0.23
5 LM	2.83	3.18	2.86	0.14	0.11	0.16

Table 4 Vertical distribution of the changes in temperature and humidity in the 11 LM experiment (Global Annual Average).

σ level	0.987	0.937	0.844	0.718	0.578	0.436	0.317	0.230
Change in temperature (°C)	2.33	2.33	2.41	2.70	3.03	3.76	4.05	3.28
Change in humidity (g/kg)	1.29	1.17	1.07	0.62	0.56	0.21	0.07	0.02
% change in humidity mixing ratio	15	16	18	21	34	35	41	56
% change in relative humidity (% of saturation)	0.1	0.3	0.2	−0.2	0.7	−1.8	−3.2	−0.8

Note. Relative humidities are calculated from seasonal averages of temperature, humidity and pressure.

Table 5 Global, annual mean changes in atmospheric heat balance (11 LM, Wm^{-2}) due to doubling CO_2 and enhancing SSTs by 2K. Note that these figures are for the atmosphere in isolation, not the combined atmosphere-surface system. The relative contributions from solar and long wavelengths are given in the second column.

		) solar	2.6
Radiative	-4.2	)	
		) longwave	-6.8
Latent	4.9		
Sensible	-0.7		

Table 6. Estimated changes in radiative fluxes and heating rates due to changes in CO_2, water vapour and temperature (Wm^{-2}). The changes diagnosed during the model simulation are given in the final column. The contributions to the longwave components were estimated by taking the annual mean profile at each grid point, running the radiation code with the changes applied one at a time, and globally averaging the results. The contributions to solar heating were estimated using a globally averaged single column model.

Radiative Component		Contribution to changes CO_2	H_2O	Temperature	All (GCM)
	Net Downward flux				
	Top	2.1	3.7	-8.8	-2.6
Longwave	Surface	1.2	5.4	-2.5	4.2
	Heating	0.9	-1.7	-6.3	-6.8
Solar	Heating	1.0	1.6	0.0	2.6
Net	Heating	1.9	-0.1	-6.3	-4.2

Table A1 Percentage area covered by grid squares where the changes in precipitation significant at the 90% level of confidence. Upper row, the difference between the anomaly and control integration; lower row, the difference between two different periods from the control integration (see Appendix). The seasons refer to the northern hemisphere: winter comprises December, January and February and so on.

SEASON	SPRING	SUMMER	AUTUMN	WINTER
% Area significant at 90% level of confidence				
Anomaly vs control	22.4	27.4	24.0	20.8
Control vs control	12.3	6.3	10.6	9.4

Table A2 Spatial correlation between P-E and changes in P-E (using annual mean data)

Correlation Coefficient		Globe	90N-30N	30N-30S	30S-90S	Tropical Oceans (30N-30S)
11LM	Uncorrected	0.36	0.48	0.33	0.61	0.39
	Corrected	0.59	0.75	0.56	0.83	0.63
5LM	Uncorrected	0.28	0.39	0.24	0.56	0.33
	Corrected	0.35	0.56	0.29	0.78	0.40

Figure Captions

Figure 1. Changes in zonally averaged atmospheric temperature in the the 11 LM due to doubling CO_2 and enhancing sea surface temperatures. Contours every 1°C, shaded where negative.

(a) June to August

(b) December to February

Figure 2. Schematic illustration of the effects of moist convective adjustment and penetrative convection schemes on an unstable (saturated) profile of wet bulb potential temperature against height (solid line). The moist convective adjustment scheme will leave a uniform θ_w profile (dashed line), with warming extending to a. The penetrative scheme considers individual convective parcels, so in principle the warming can penetrate to b. The final profile (not shown) will be warmer at upper levels and cooler at lower levels than in the case of convective adjustment.

Figure 3. Changes in zonally averaged relative humidity in the 11 LM (calculated from seasonal averages of temperature, pressure and humidity) due to doubling CO_2 and enhancing sea surface temperatures. Contours every 2%, shaded where negative.

a. June to August.

b. December to February.

Figure 4. Changes in zonally averaged west to east wind in the 11 LM due to doubling CO_2 and enhancing sea surface temperatures. Contours every 1 m/s, shaded where negative. Dashed lines indicate the latitudes of maximum west to east wind in the control integration.

(a) June to August

(b) December to February

Figure 5. As Figure 1, but for the 5 LM.

Figure 6. As Figure 4, but for the 5 LM.

Figure 7. Zonally averaged precipitation from the control (solid line) and anomaly integrations (dashed line), and differences (dotted line) in the 11 layer model (mm/day).

(a) June to August

(b) December to February

Figure 8. As 7, but for the 5 LM. (Note that in Mitchell (1983), the seasons are incorrectly labelled in Figure 9).

Figure 9. Geographical distribution of precipitation changes in the 11 LM due to doubling CO_2 and enhancing sea surface temperatures. Contours and -2, -1, 0, 1 and 2 mm/day, areas of decrease shaded.

(a) June to August

(b) December to February

Figure 10. Precipitation from control integration of the 11 LM (8 year mean). Contours at 1, 2, 5, 10, 20 and 40 mm/day, stippled where greater than 5 mm/day.

(a) June to August

(b) December to February

Figure 11. As for 9, but from the 5 LM.

Figure 12. Precipitation from the control integration of the 5 LM (3 year mean). Contours at 1, 2, 5, and 10 mm/day. Lightly stippled where less than 1 mm/day, heavily stippled where greater than 5 mm/day and solid where greater than 10 mm/day.

(a) June to August

(b) December to February

Figure 13. Student's t-tests on differences in precipitation in the 11LM experiment (3 years data from the anomaly integration; 8 years from the control). A two-sided test has been used, allowing 9 degrees of freedom, and grid boxes with changes which would occur by chance on less than ten per cent of occasions are stippled. Areas of significant increase are stippled heavily, areas of decrease are stippled lightly. Also shown are the standard deviations of the seasonal mean for the control integration. Solid contours at 1, 5 mm/day, chain dotted contour at 2 mm/day.

(a) June to August

(b) December to February

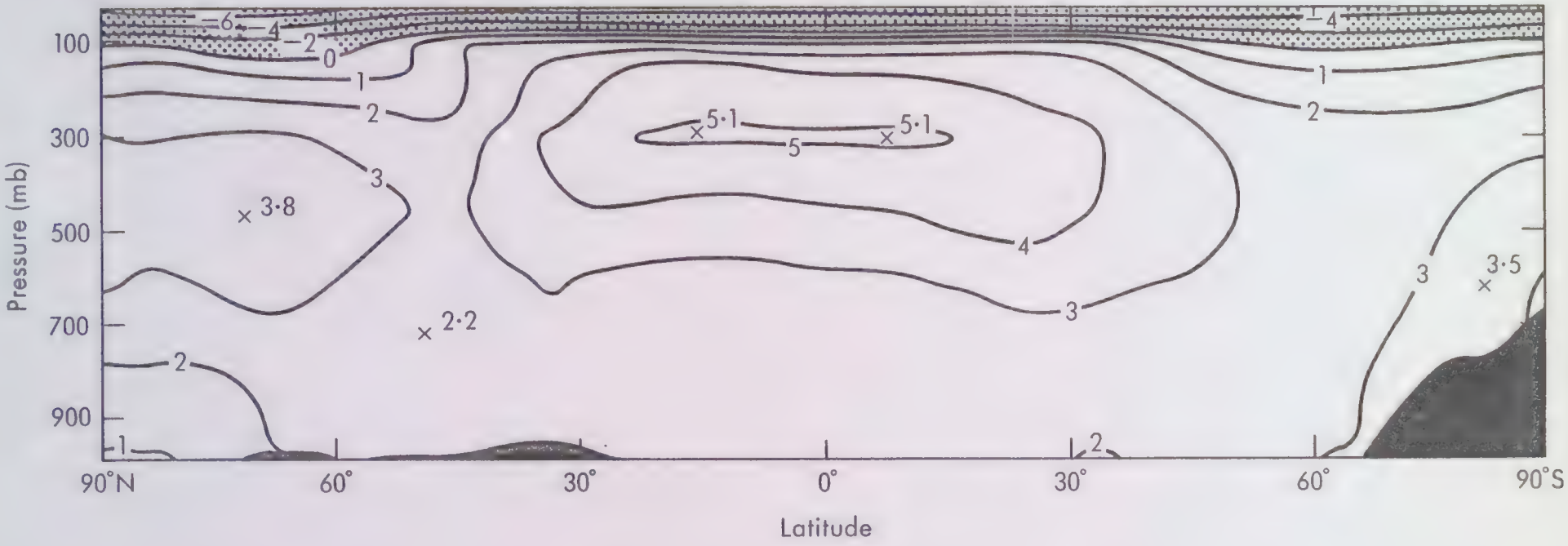
Pressure (mb)
100
300
500
700
900
−6
−4
−2
0
1
2
3
4
5
5·1
5·1
3·8
2·2
3·5
90°N
60°
30°
0°
30°
60°
90°S
Latitude

Figure 1a

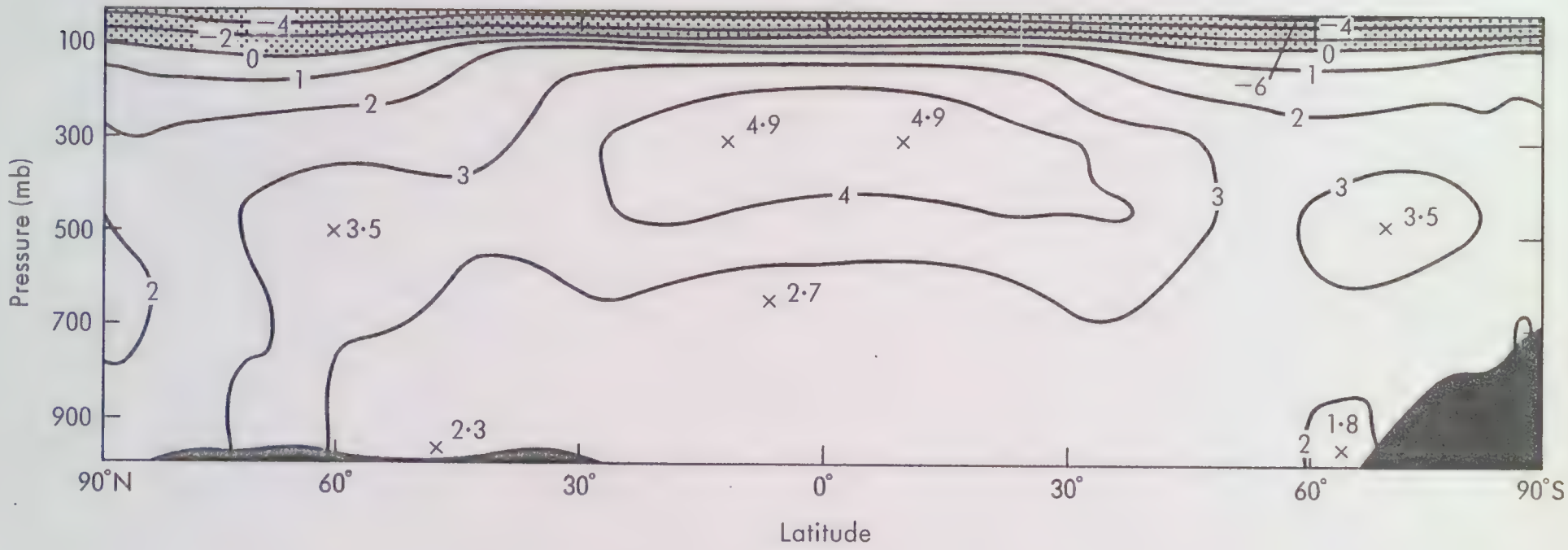
100
300
500
700
900
Pressure (mb)
−4
−2
0
1
2
3
4
−6
4·9
4·9
3·5
2·7
3·5
2·3
1·8
90°N
60°
30°
0°
30°
60°
90°S
Latitude

Figure 1b

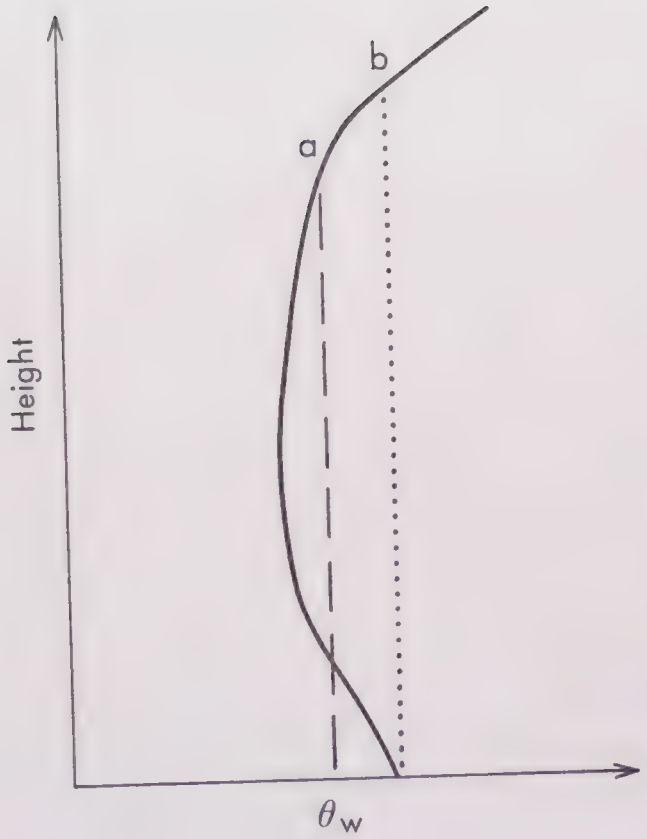

Figure 2

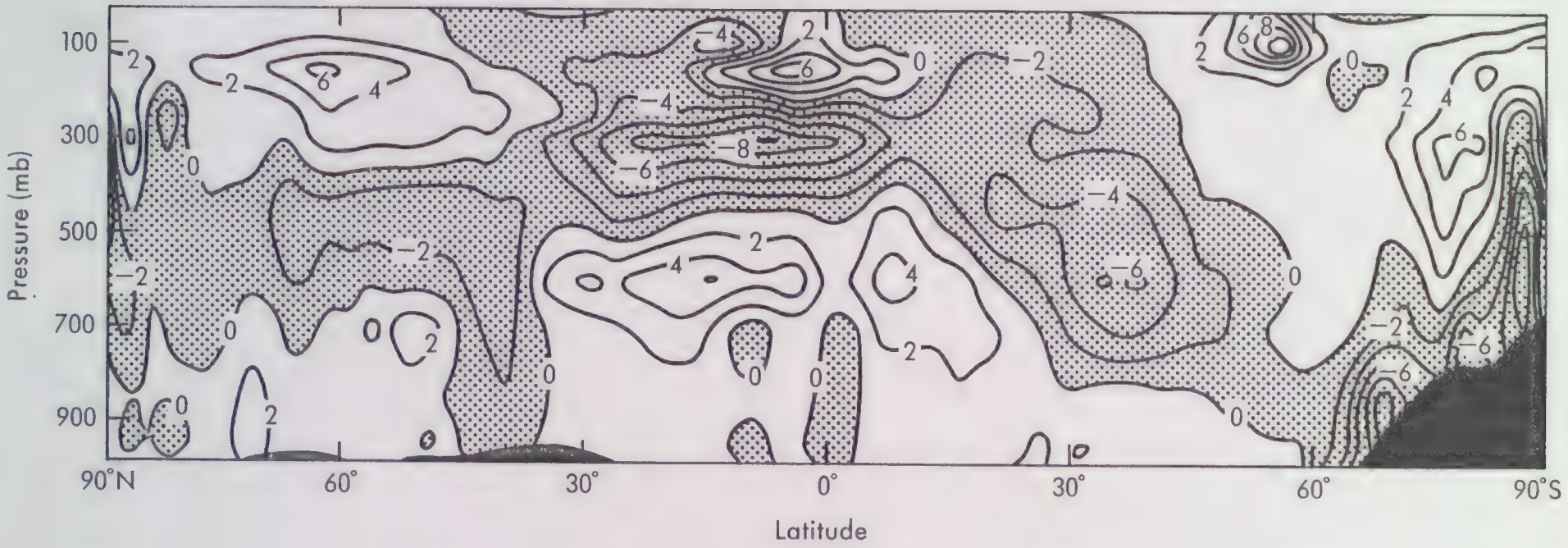

Figure 3a

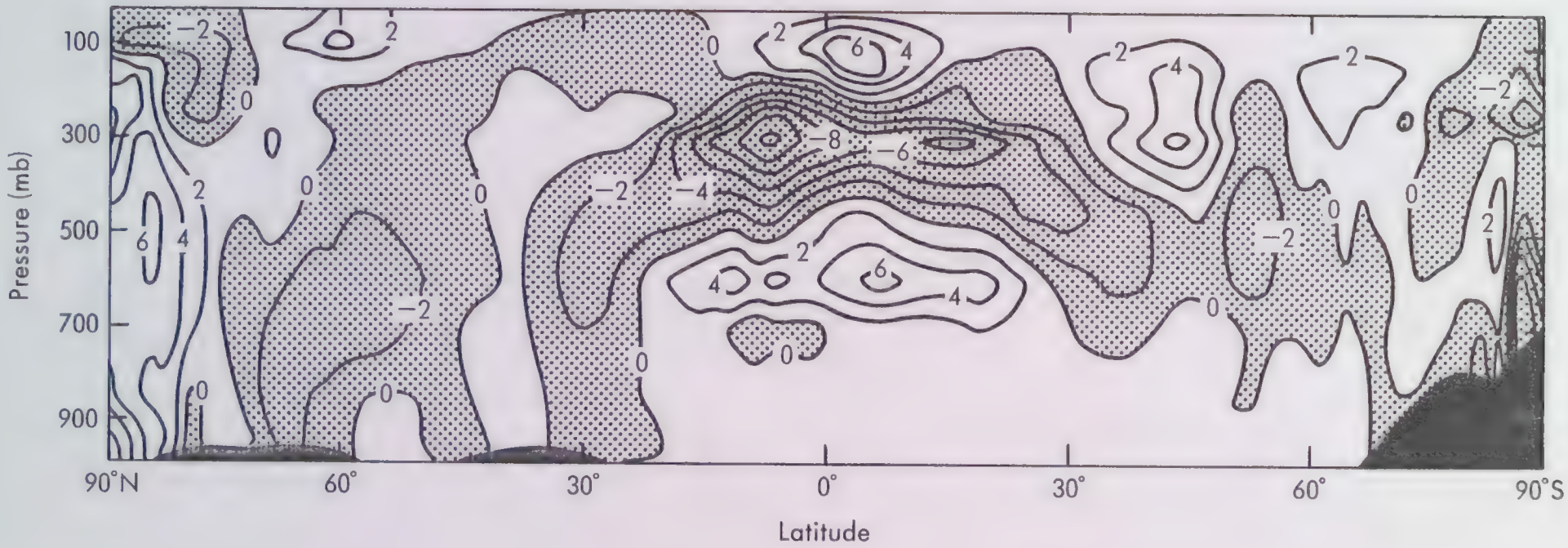

Figure 3b

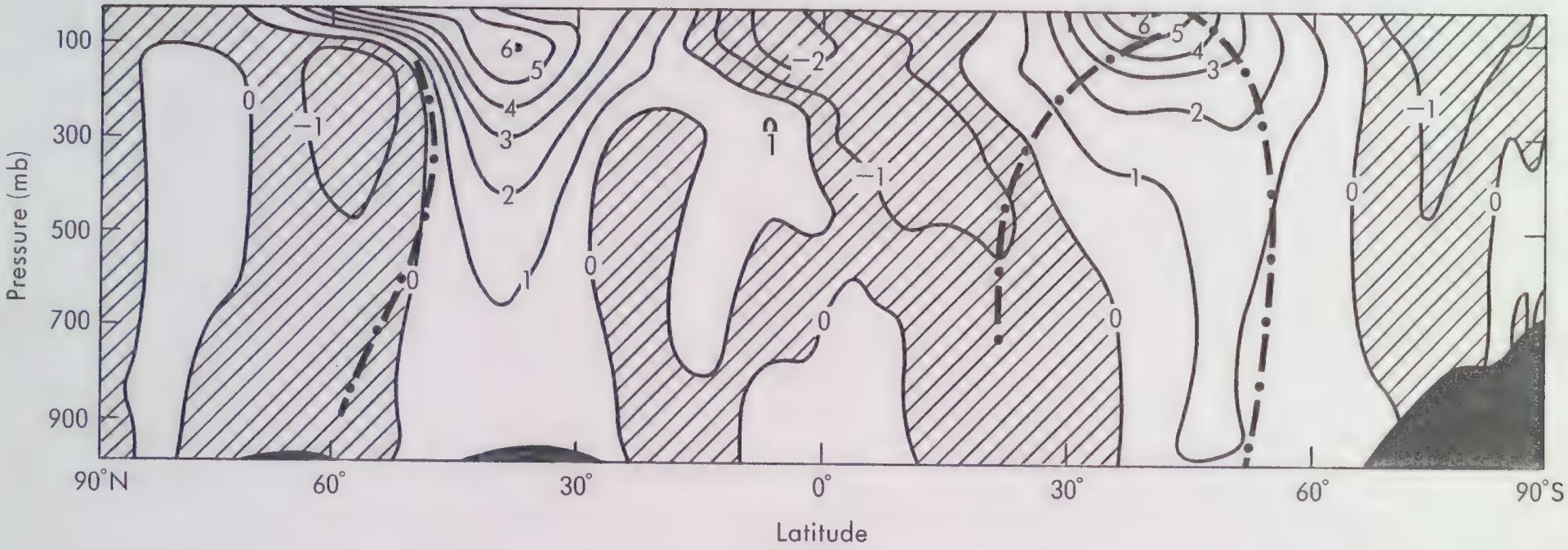
Pressure (mb)
100
300
500
700
900
90°N
60°
30°
0°
30°
60°
90°S
Latitude
6
5
4
3
2
1
0
−1
−2

Figure 4a

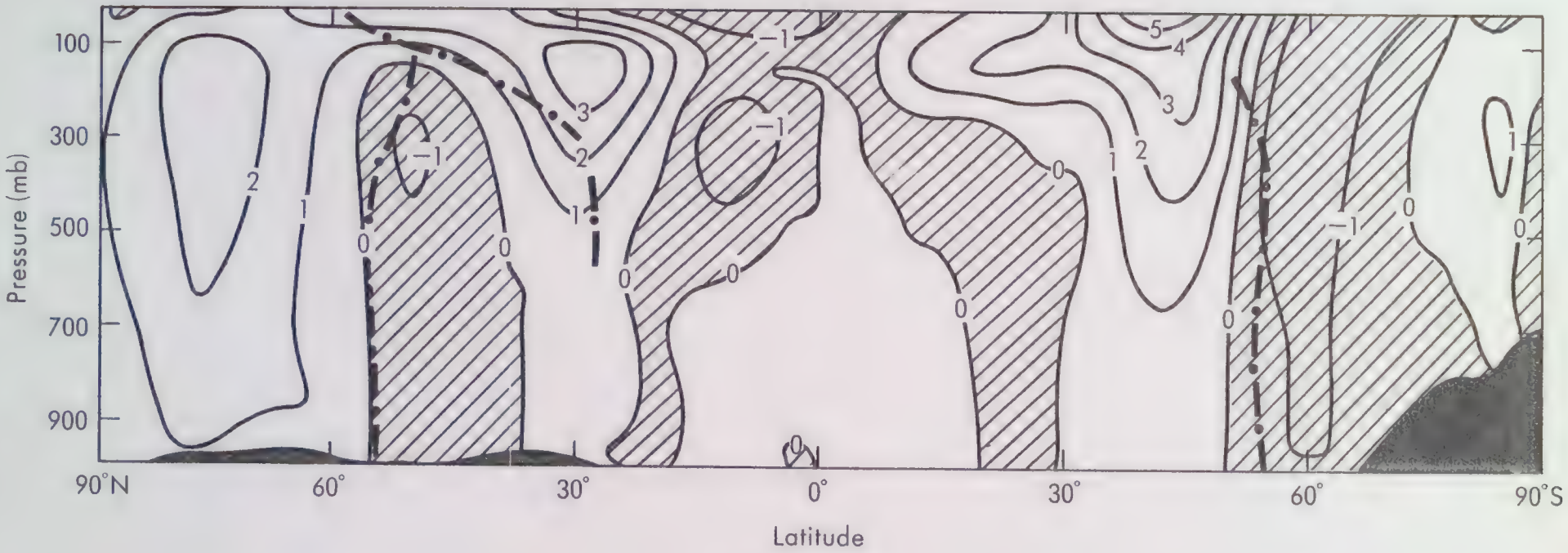

Figure 4b

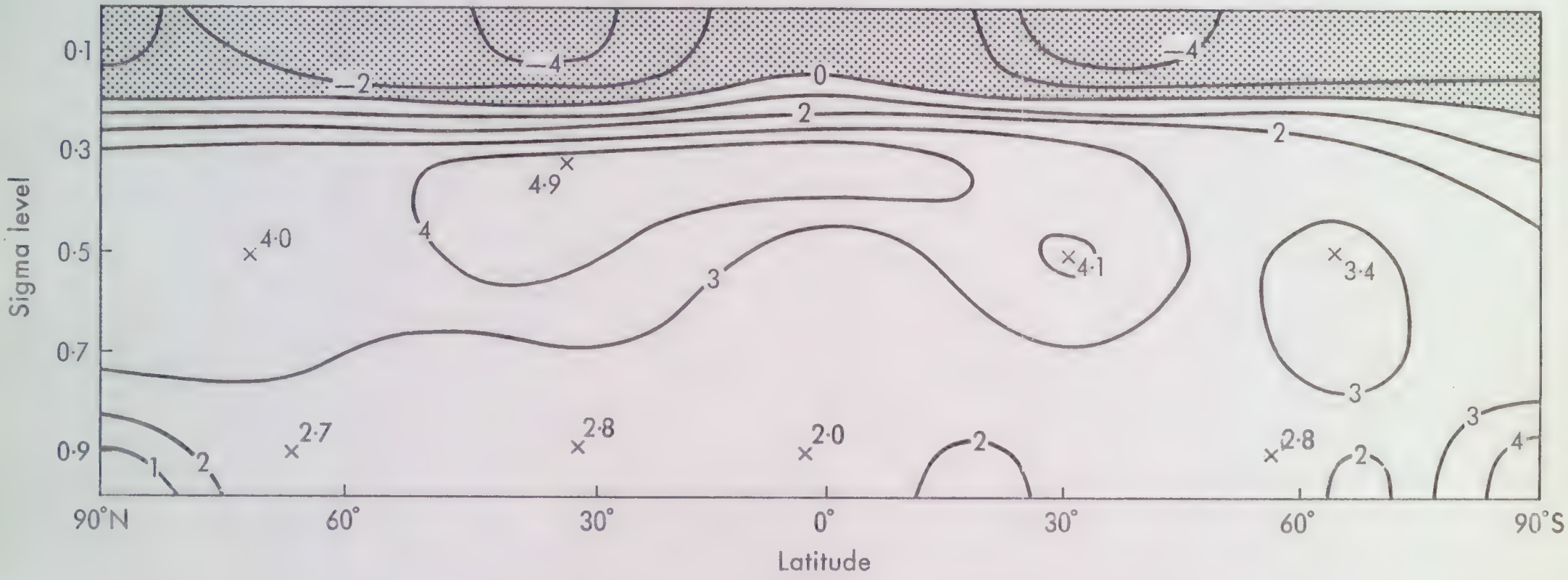
0·1
0·3
0·5
0·7
0·9
Sigma level
−4
−2
0
2
2
−4
4·9
4·0
4
3
4·1
3·4
3
2·7
2·8
2·0
2
2·8
2
3
4
1
2
90°N
60°
30°
0°
30°
60°
90°S
Latitude

Figure 5a

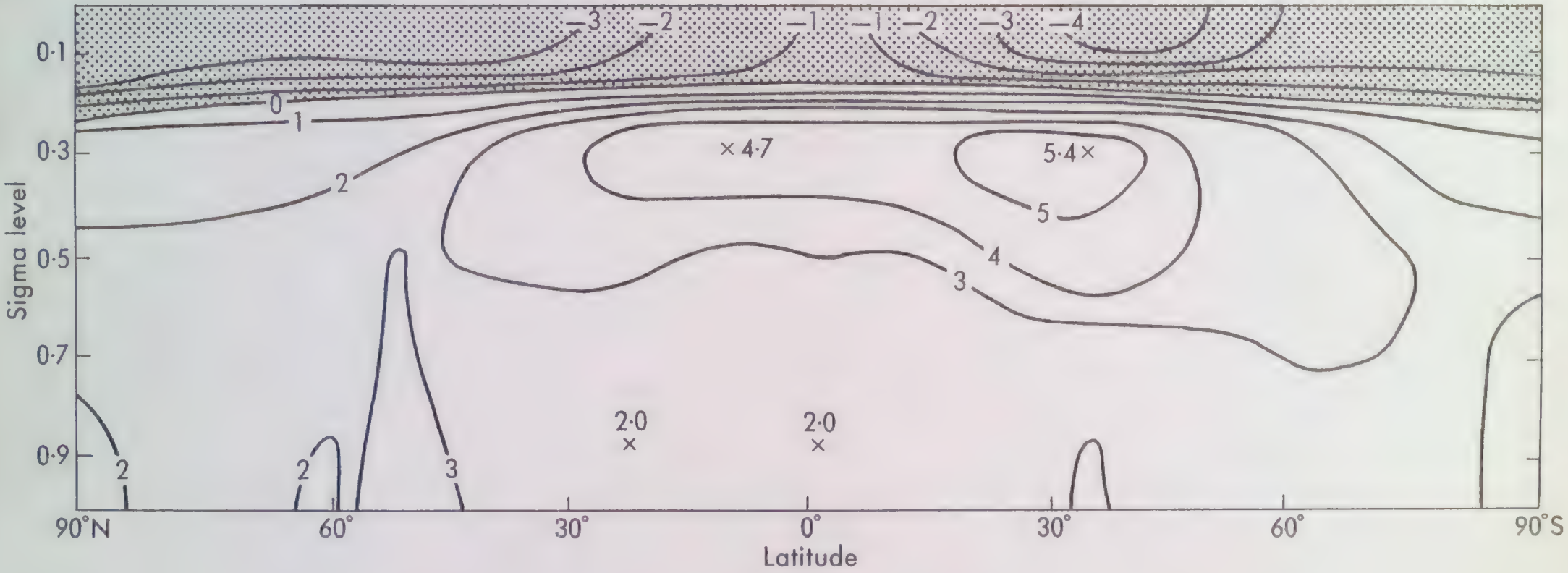
−3
−2
−1
−1
−2
−3
−4
0·1
0
1
0·3
2
× 4·7
5·4 ×
5
4
3
Sigma level
0·5
0·7
2·0
×
2·0
×
0·9
2
2
3
90°N
60°
30°
0°
30°
60°
90°S
Latitude

Figure 5b

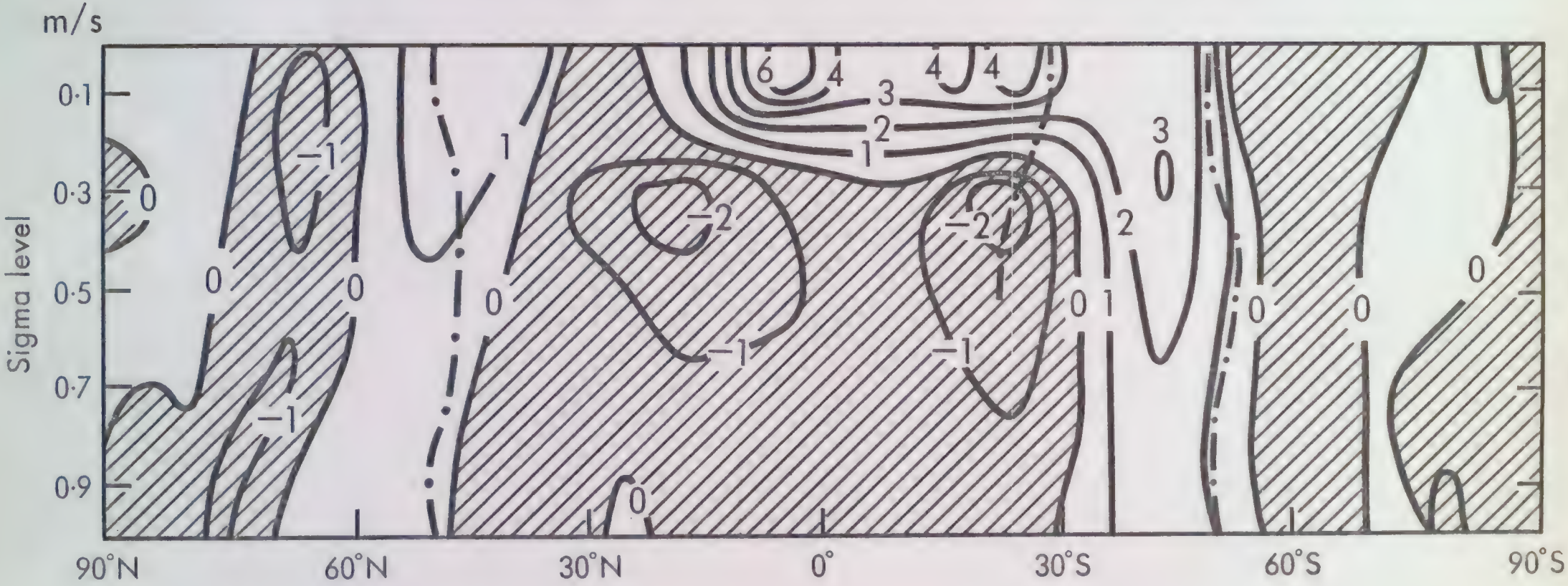

Figure 6a

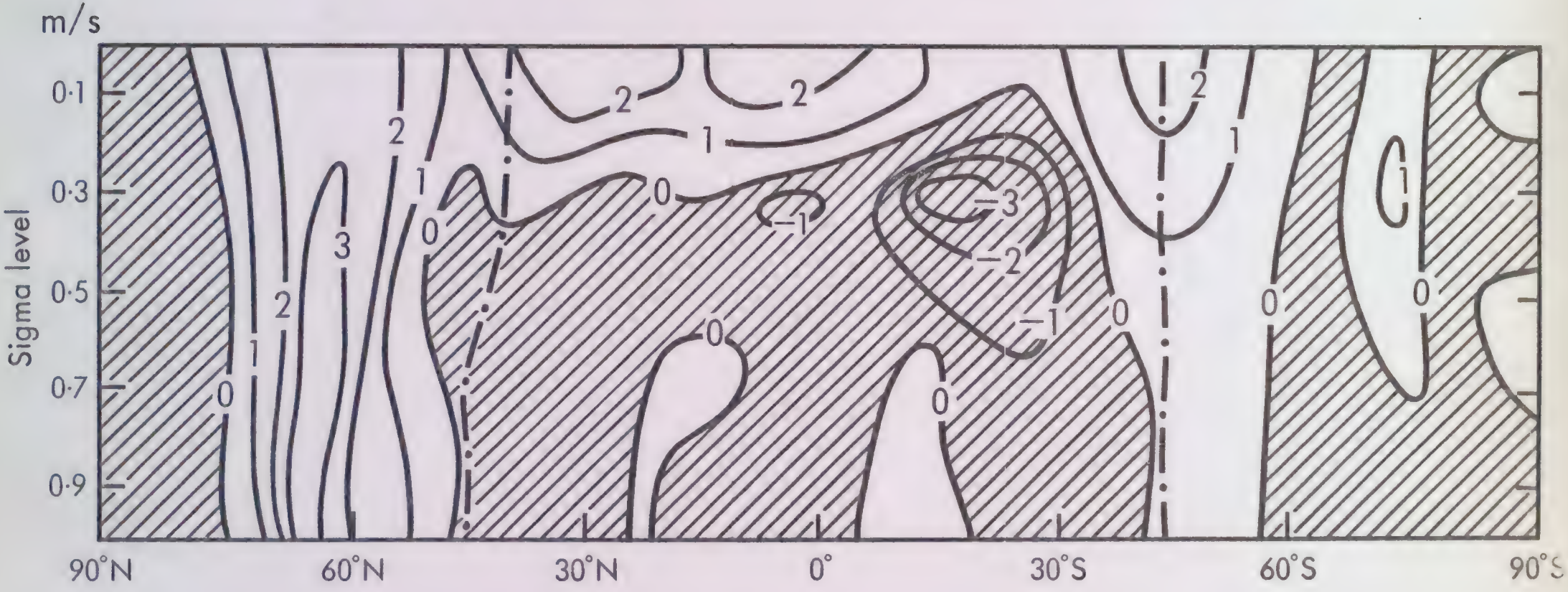

Figure 6b

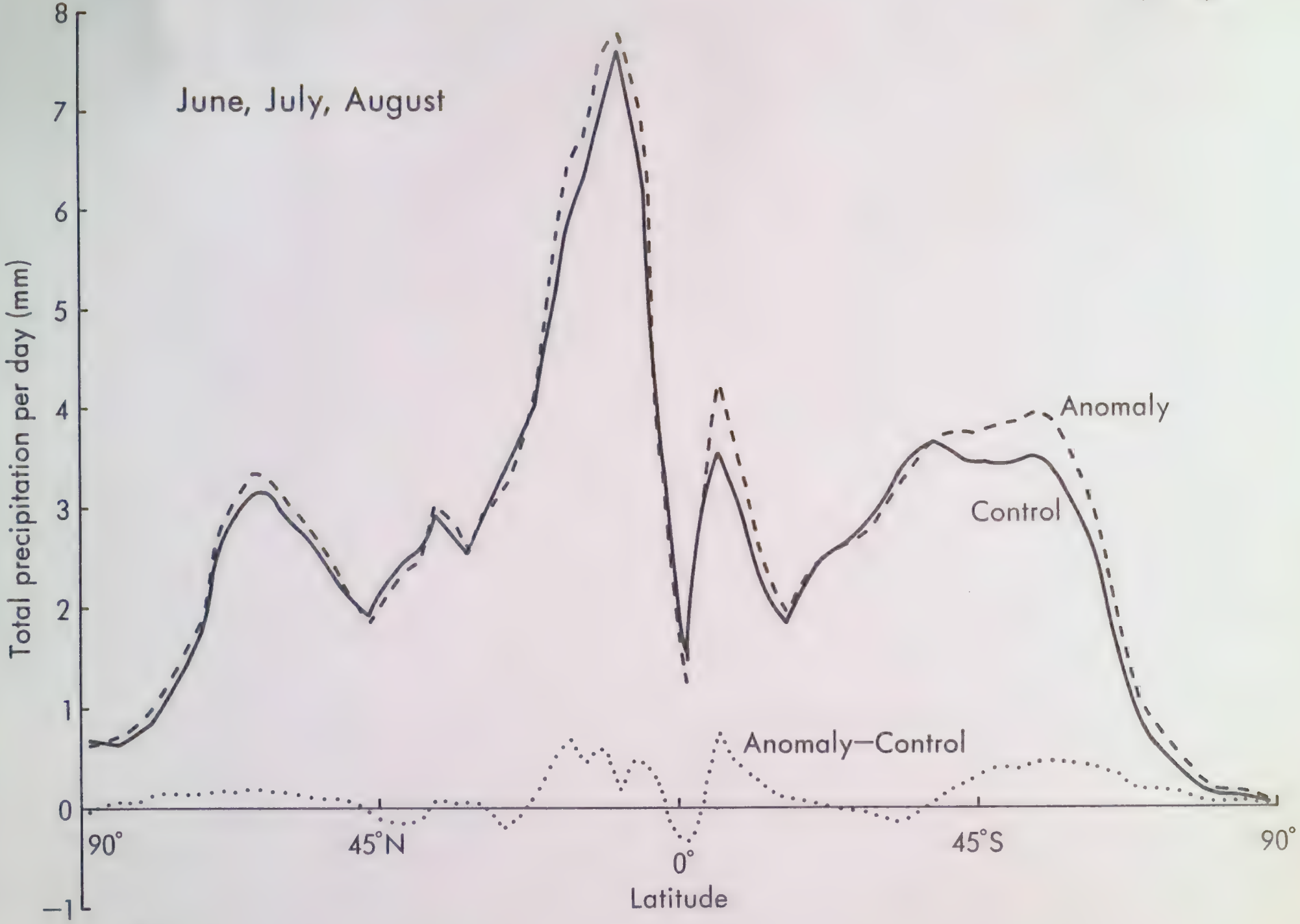
June, July, August
Total precipitation per day (mm)
8
7
6
5
4
3
2
1
0
−1
Anomaly
Control
Anomaly—Control
90°
45°N
0°
45°S
90°
Latitude

Figure 7a

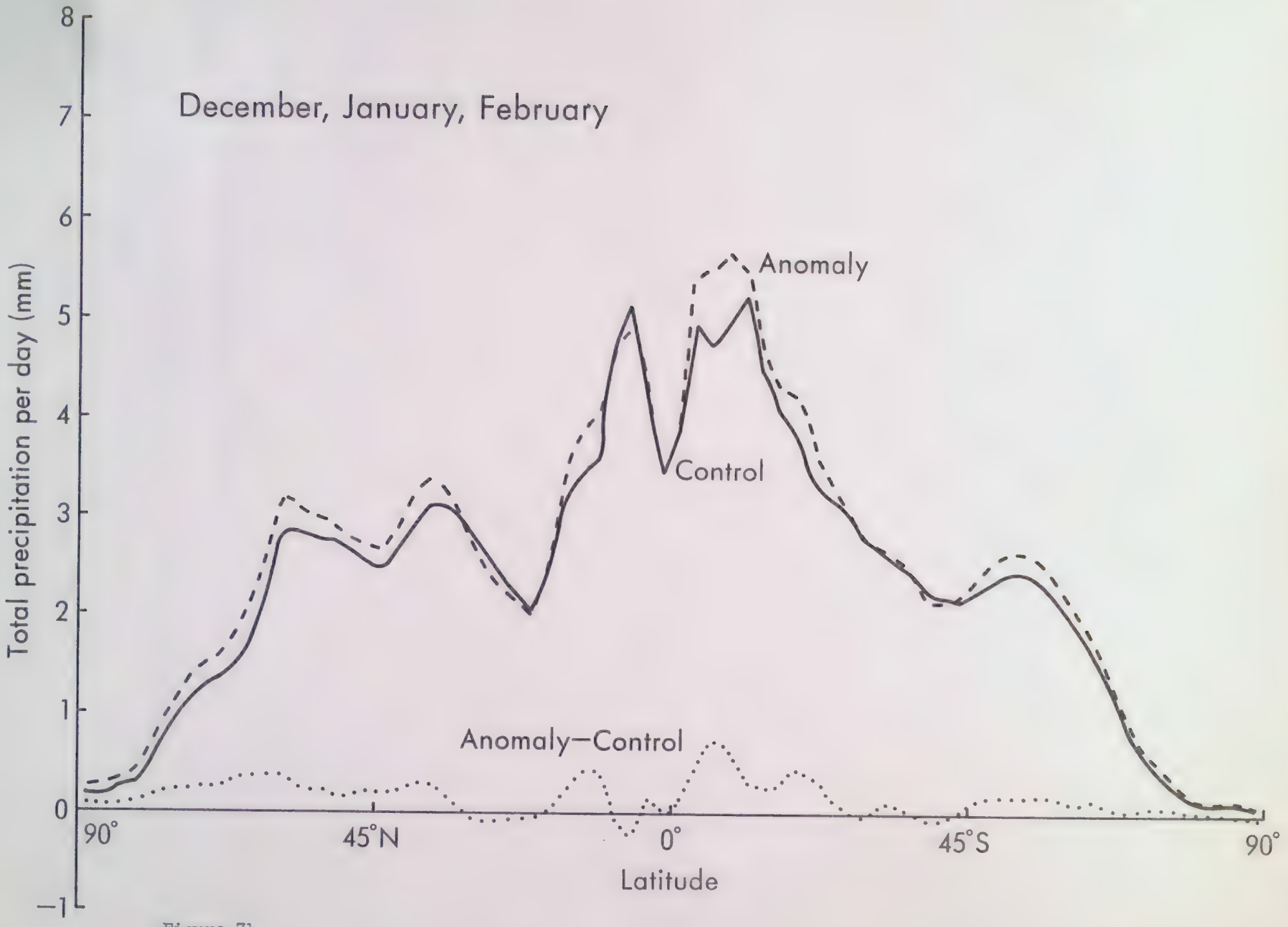
December, January, February
Total precipitation per day (mm)
8
7
6
5
4
3
2
1
0
−1
Anomaly
Control
Anomaly−Control
90°
45°N
0°
45°S
90°
Latitude

Figure 7b

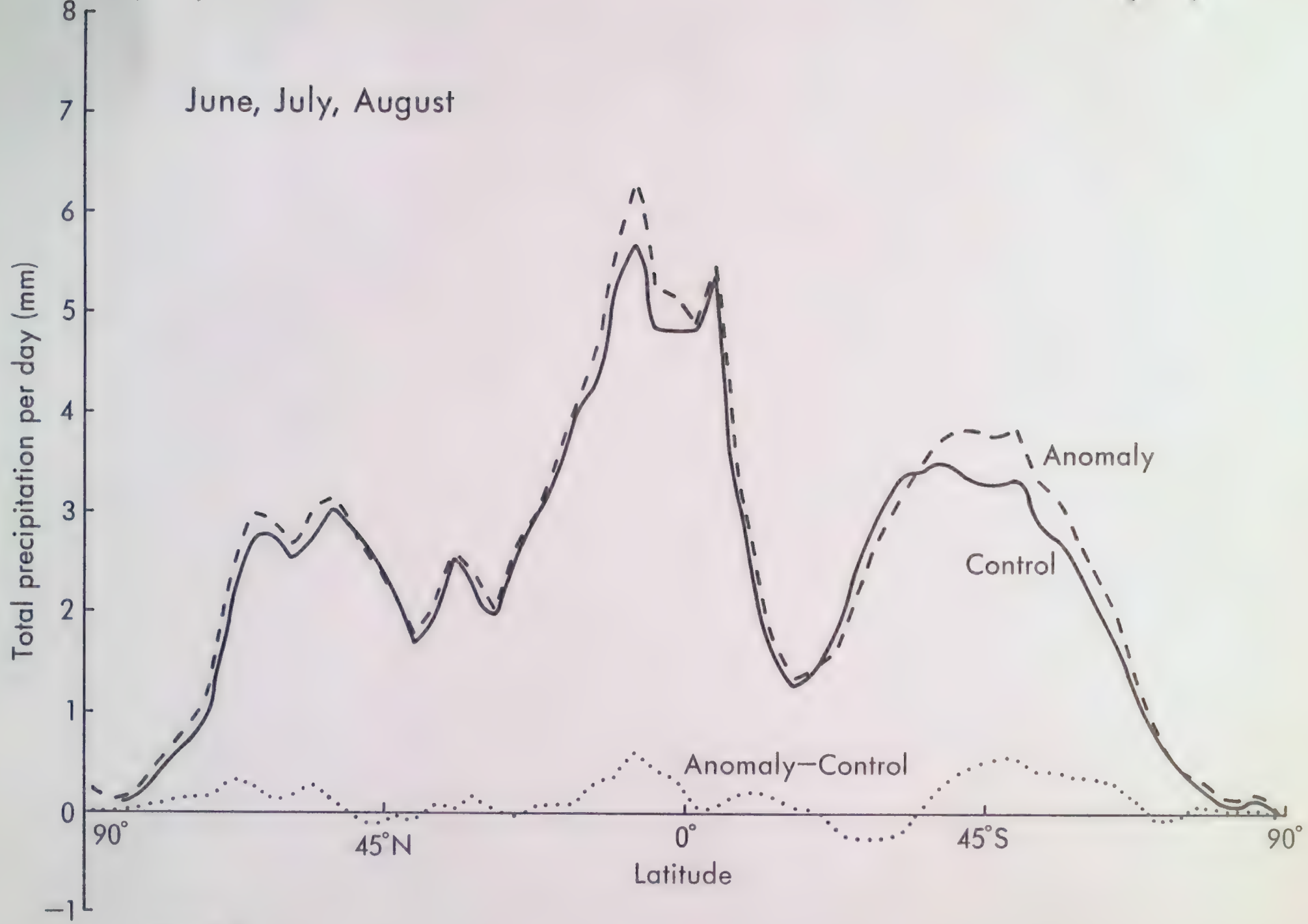
June, July, August
Total precipitation per day (mm)
8
7
6
5
4
3
2
1
0
−1
Anomaly
Control
Anomaly—Control
90°
45°N
0°
45°S
90°
Latitude

Figure 8a

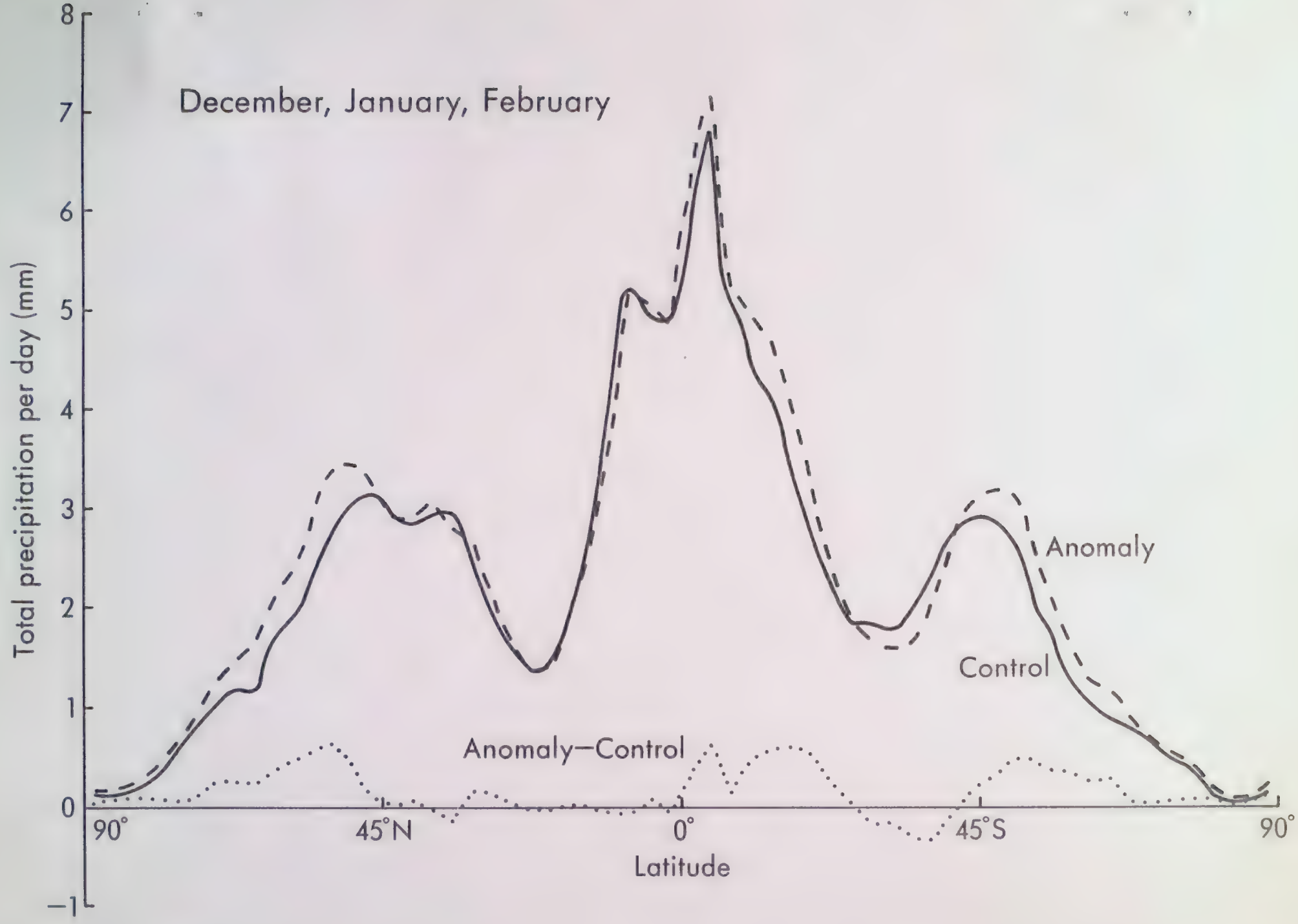
December, January, February
Total precipitation per day (mm)
8
7
6
5
4
3
2
1
0
−1
Anomaly
Control
Anomaly—Control
90°
45°N
0°
45°S
90°
Latitude

Figure 8b

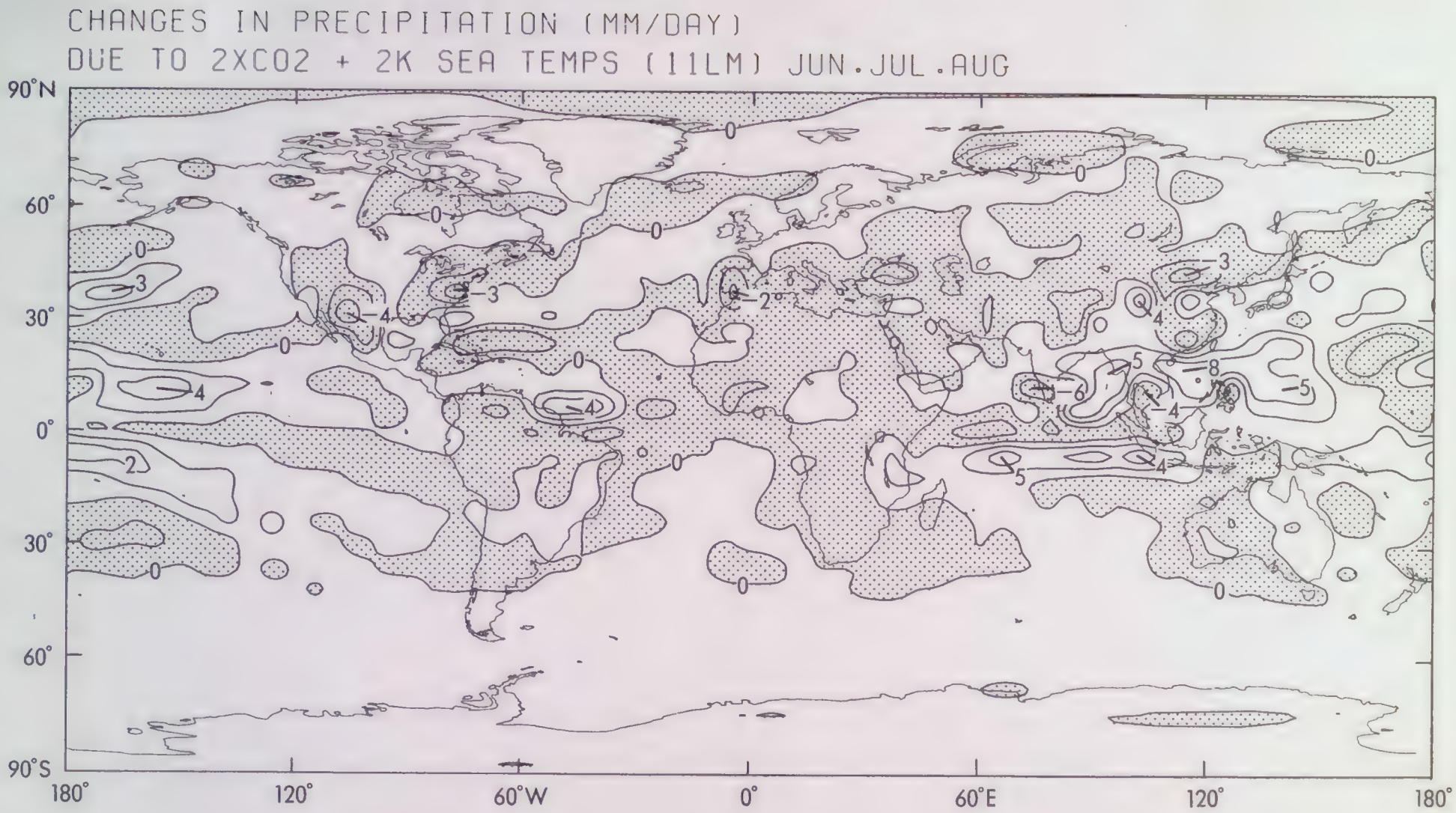
CHANGES IN PRECIPITATION (MM/DAY)
DUE TO 2XCO2 + 2K SEA TEMPS (11LM) JUN.JUL.AUG
90°N
60°
30°
0°
30°
60°
90°S
180°
120°
60°W
0°
60°E
120°
180°

Figure 9a

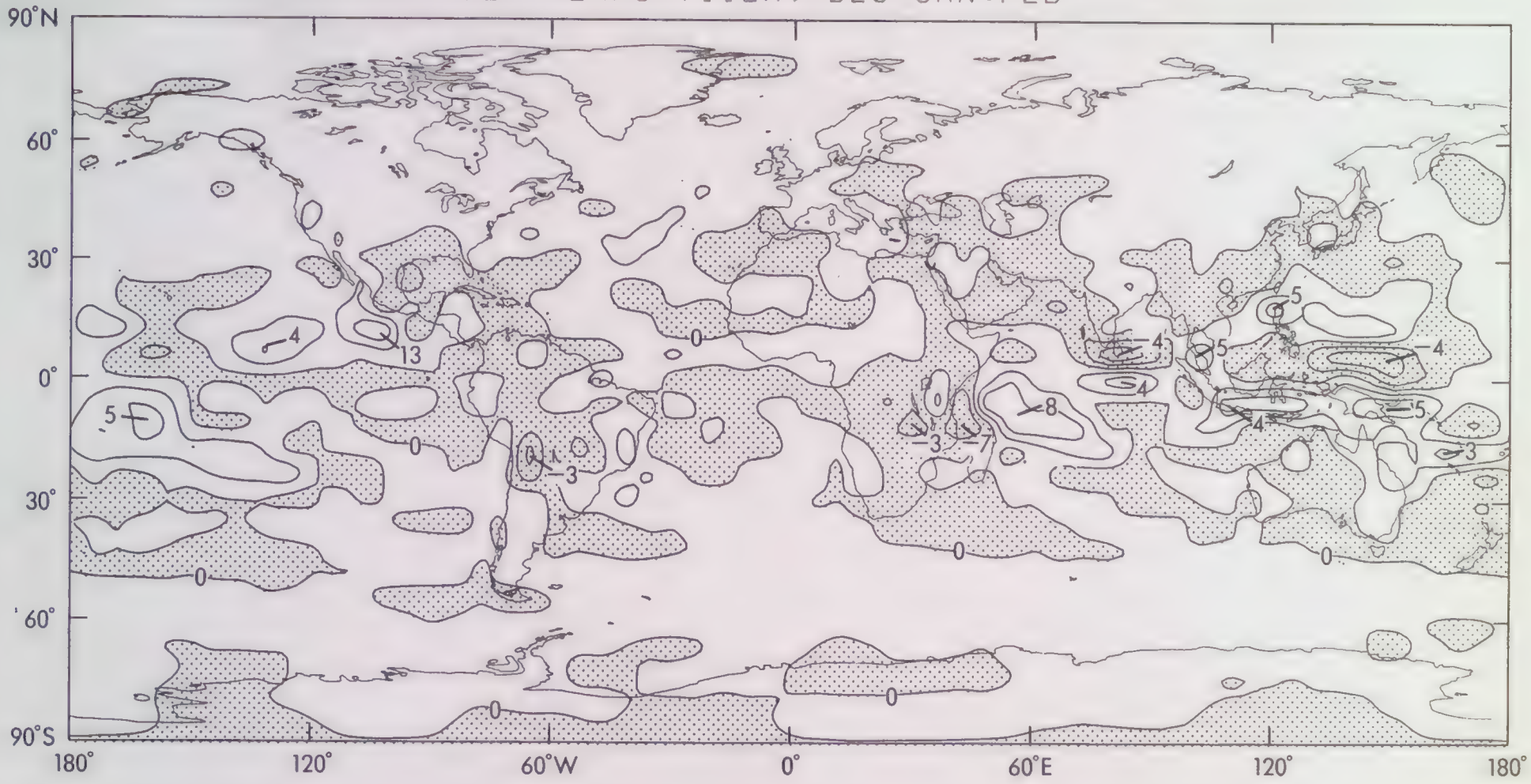
CHANGES IN PRECIPITATION (MM/DAY)
DUE TO 2XCO2 + 2K SEA TEMPS (11LM) DEC.JAN.FEB
90°N
60°
30°
0°
30°
60°
90°S
180°
120°
60°W
0°
60°E
120°
180°

Figure 9b

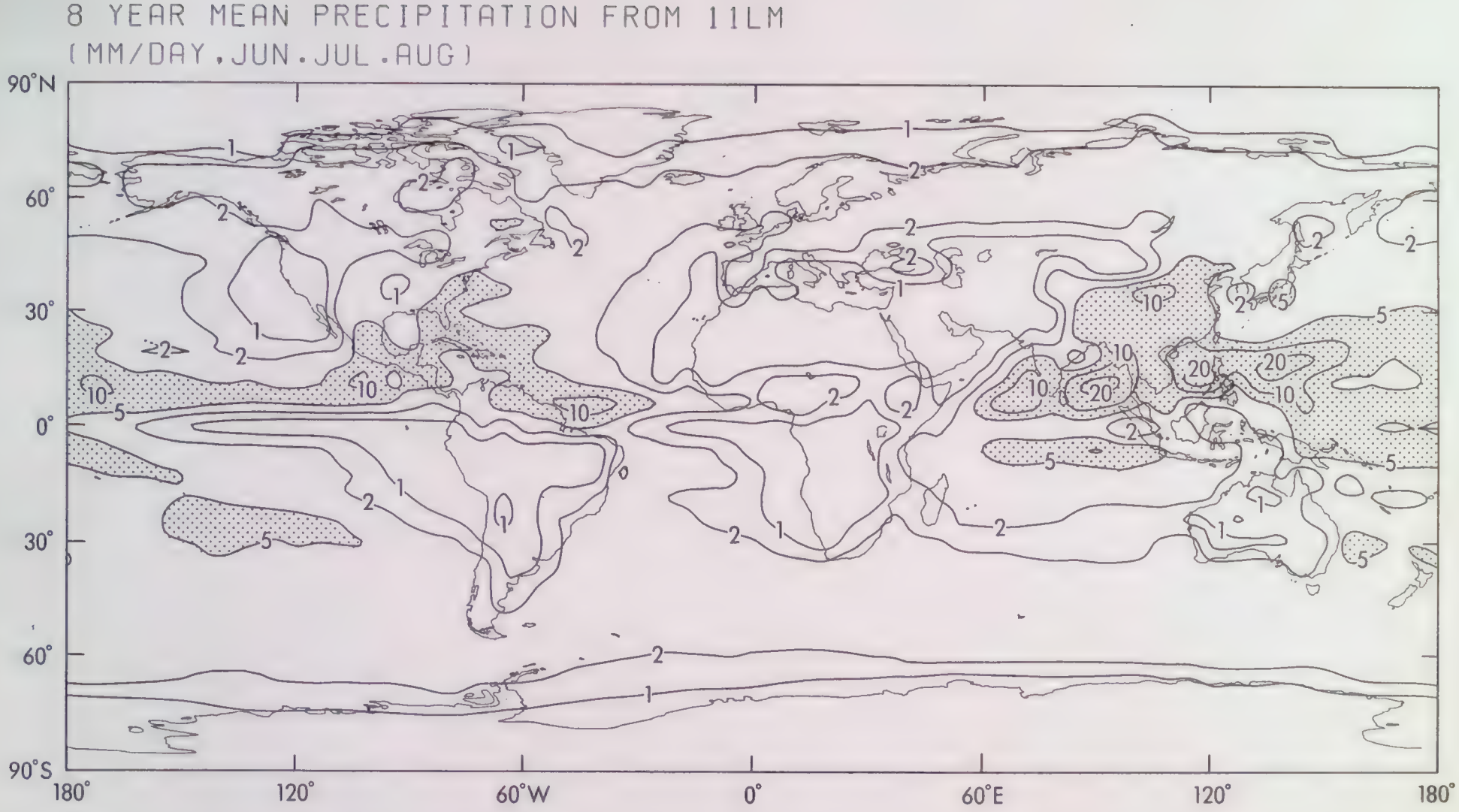
8 YEAR MEAN PRECIPITATION FROM 11LM
(MM/DAY,JUN.JUL.AUG)
90°N
60°
30°
0°
30°
60°
90°S
180°
120°
60°W
0°
60°E
120°
180°

Figure 10a

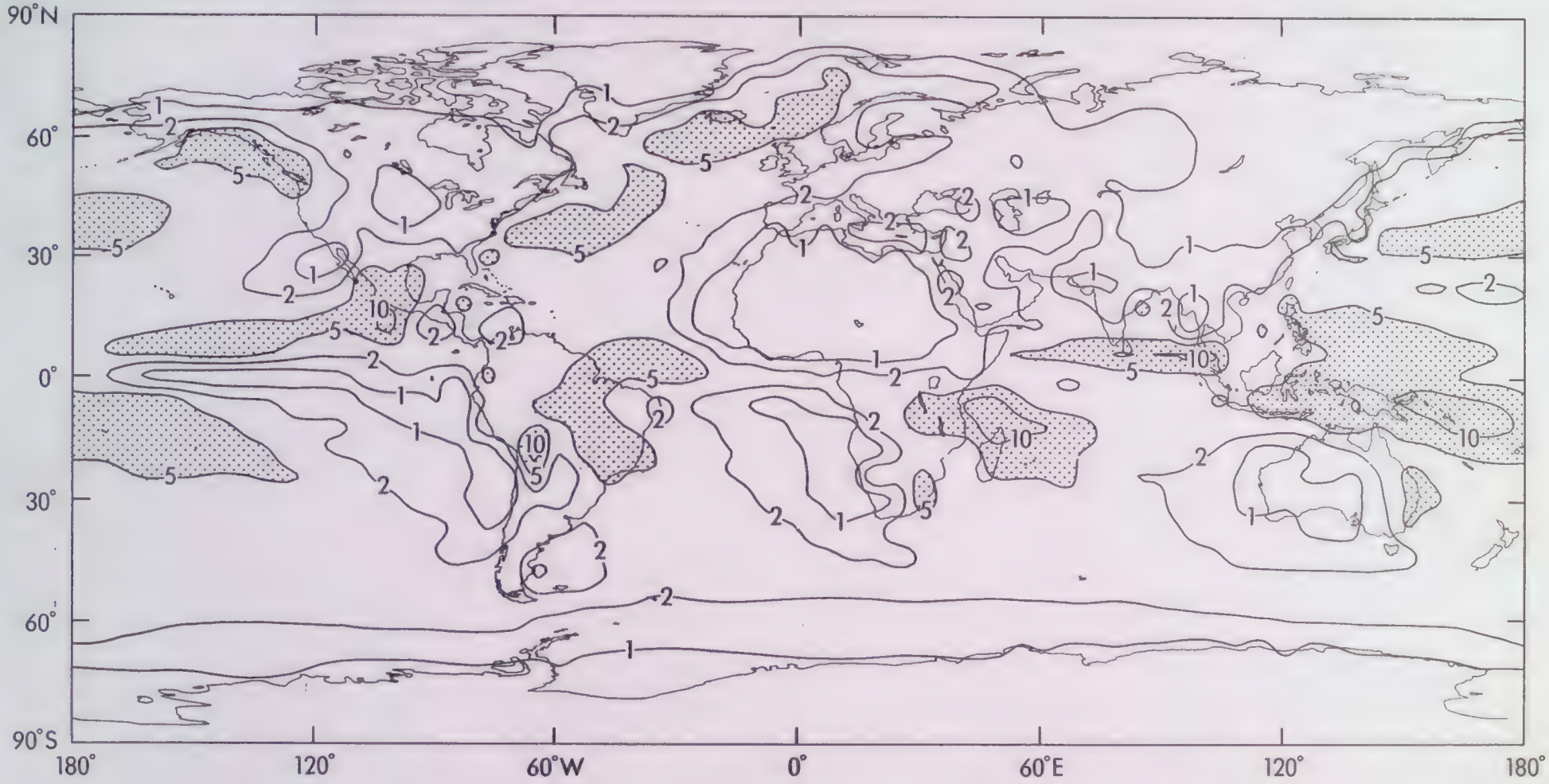
8 YEAR MEAN PRECIPITATION FROM 11LM
(MM/DAY.DEC.JAN.FEB)
90°N
60°
30°
0°
30°
60°
90°S
180°
120°
60°W
0°
60°E
120°
180°

Figure 10b

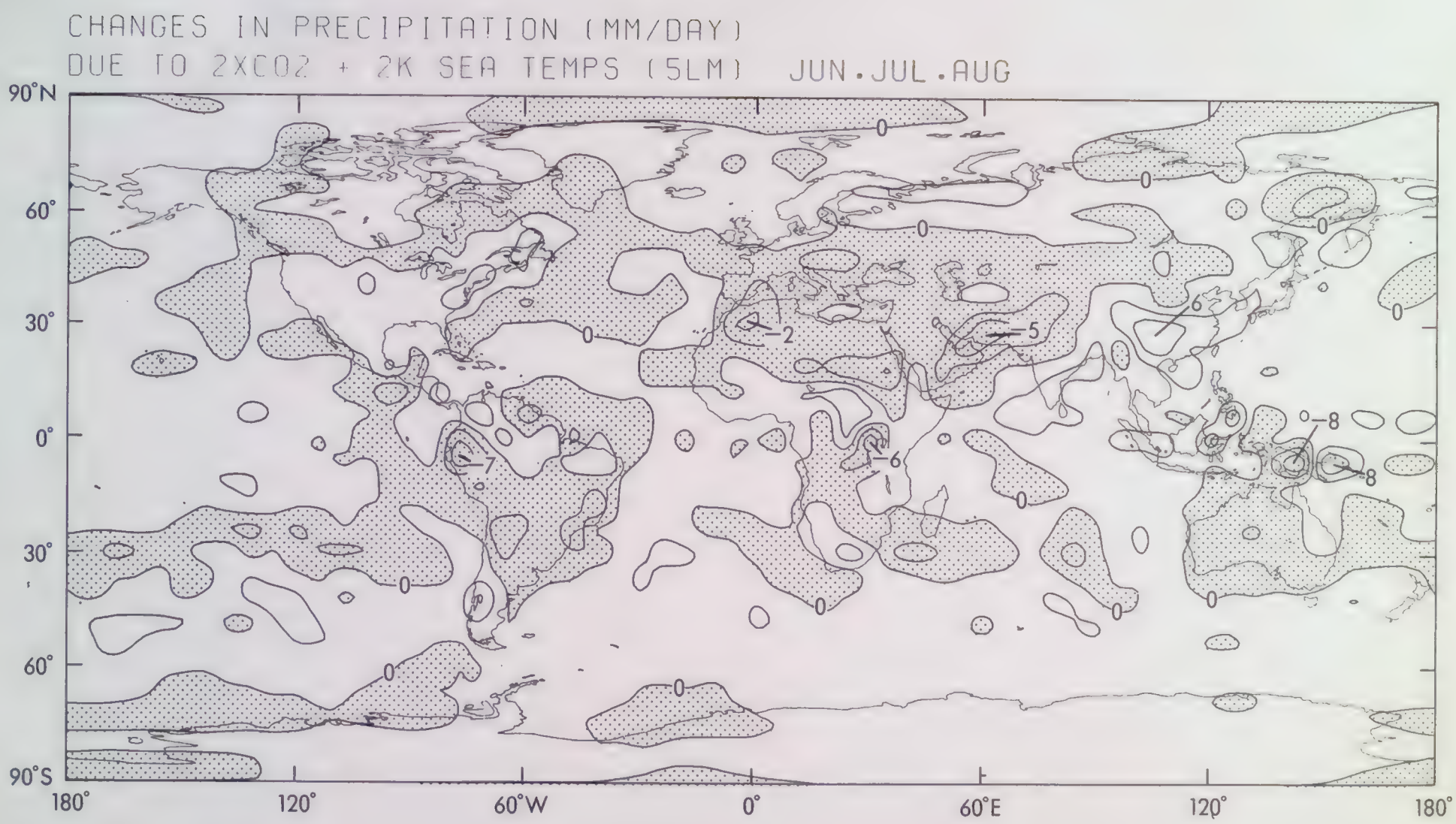
CHANGES IN PRECIPITATION (MM/DAY)
DUE TO 2XCO2 + 2K SEA TEMPS (5LM) JUN.JUL.AUG
90°N
60°
30°
0°
30°
60°
90°S
180°
120°
60°W
0°
60°E
120°
180°
0
−2
−5
6
−8
−7
−6
8

Figure 11a

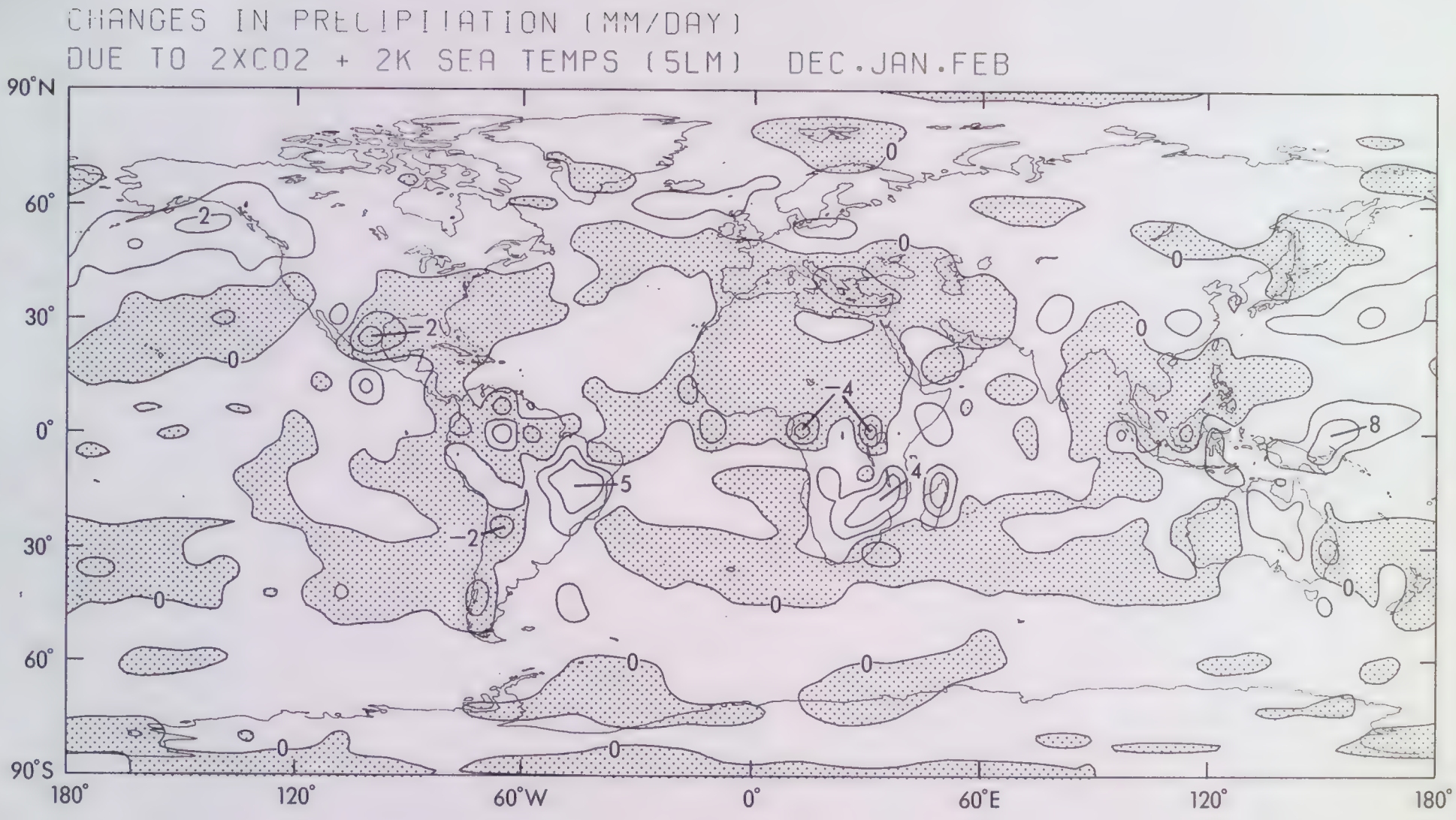
CHANGES IN PRECIPITATION (MM/DAY)
DUE TO 2XCO2 + 2K SEA TEMPS (5LM) DEC.JAN.FEB
90°N
60°
30°
0°
30°
60°
90°S
180°
120°
60°W
0°
60°E
120°
180°
0
2
-2
-4
4
5
8

Figure 11b

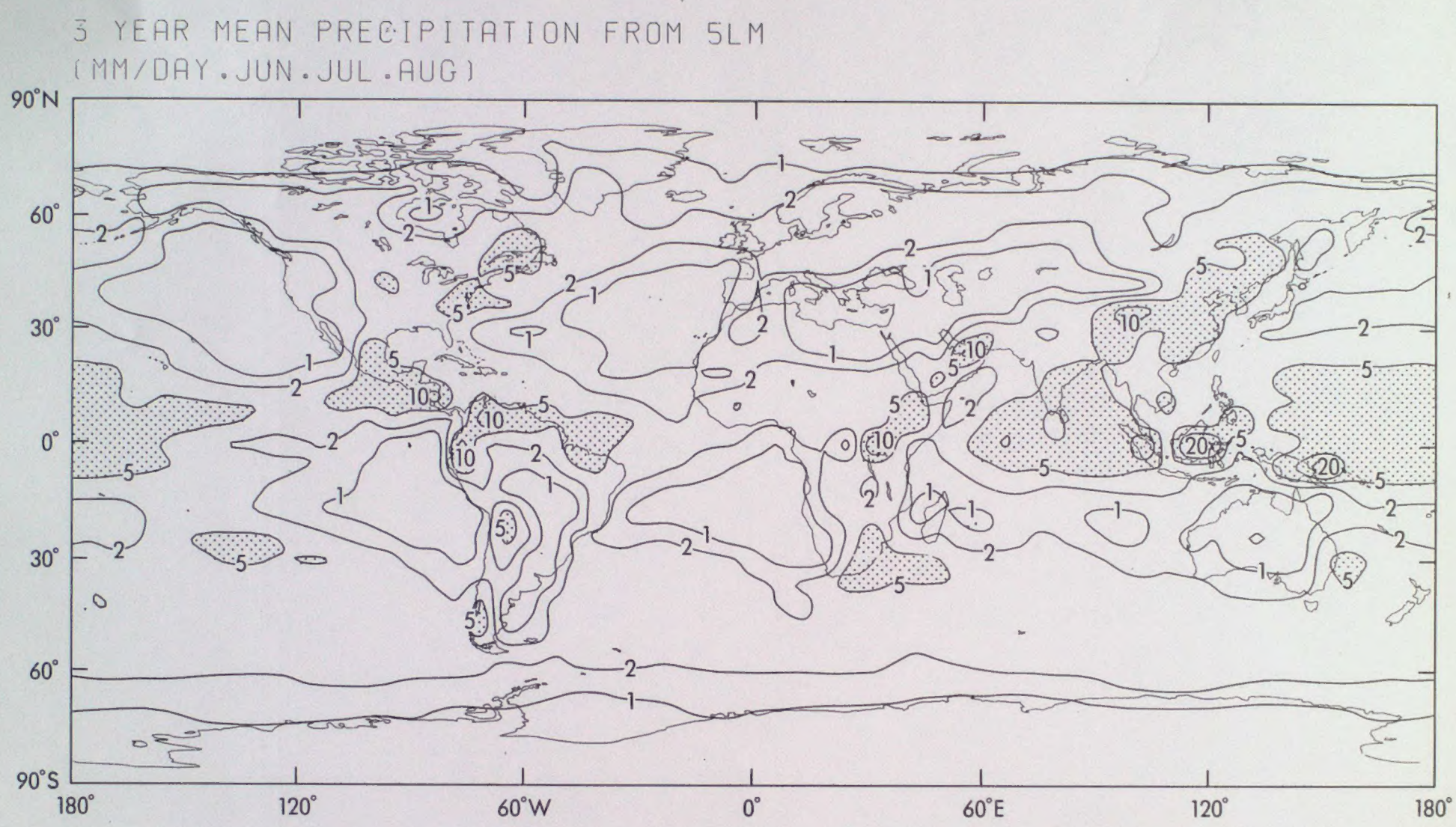
3 YEAR MEAN PRECIPITATION FROM 5LM
(MM/DAY.JUN.JUL.AUG)
90°N
60°
30°
0°
30°
60°
90°S
180°
120°
60°W
0°
60°E
120°
180°

Figure 12a

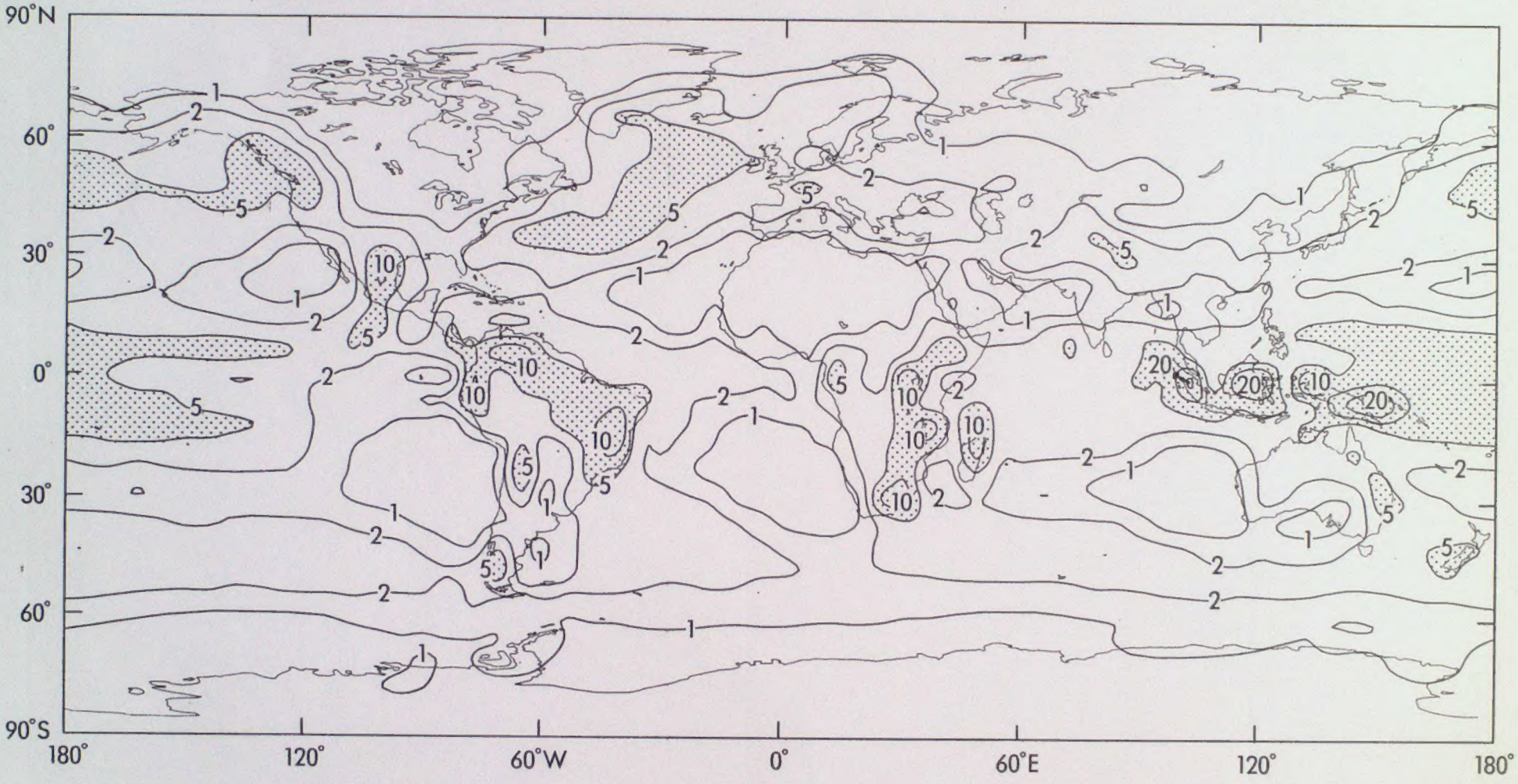
3 YEAR MEAN PRECIPITATION FROM 5LM
(MM/DAY.DEC.JAN.FEB)
90°N
60°
30°
0°
30°
60°
90°S
180°
120°
60°W
0°
60°E
120°
180°

Figure 12b

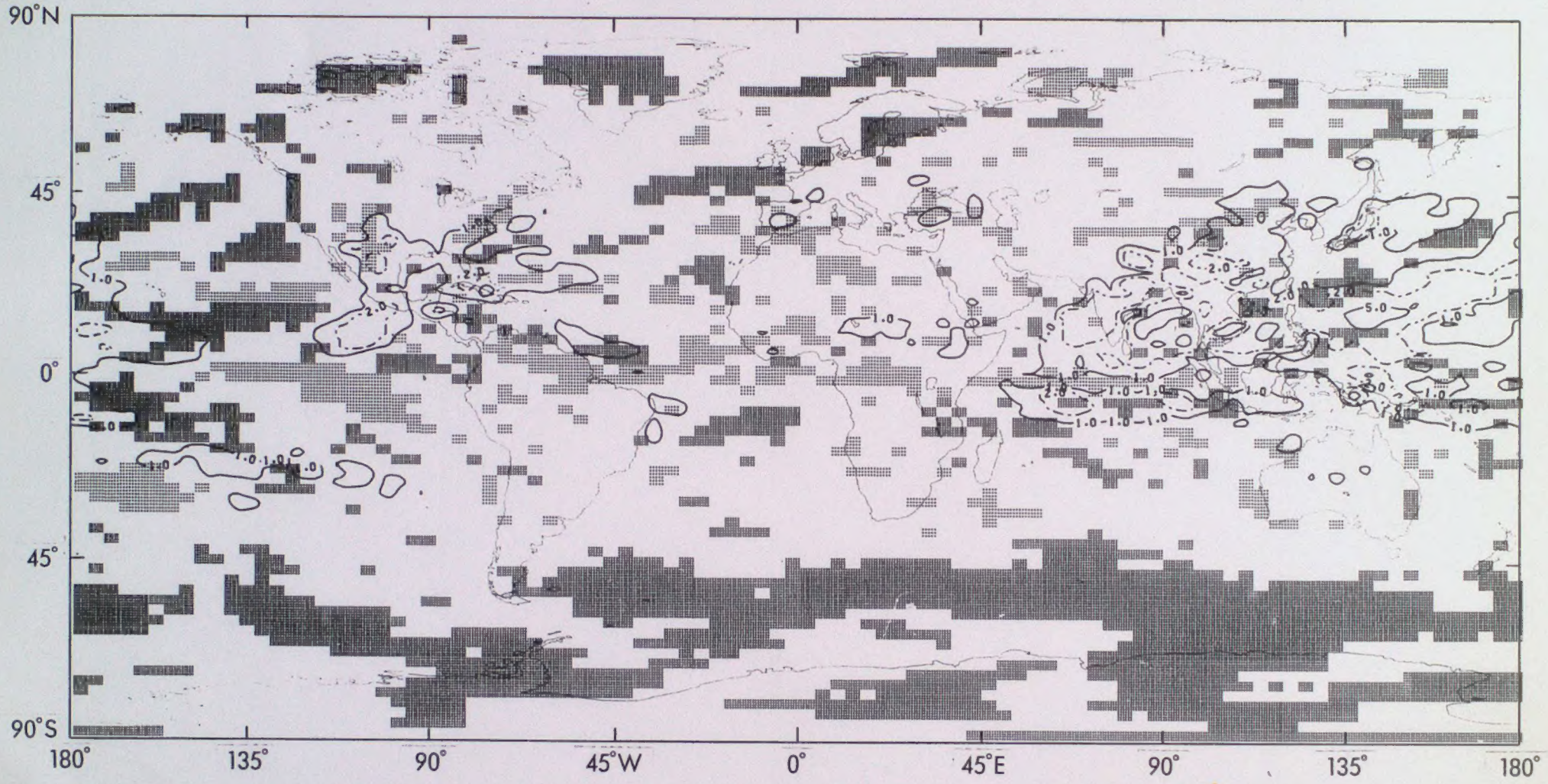

Figure 13a

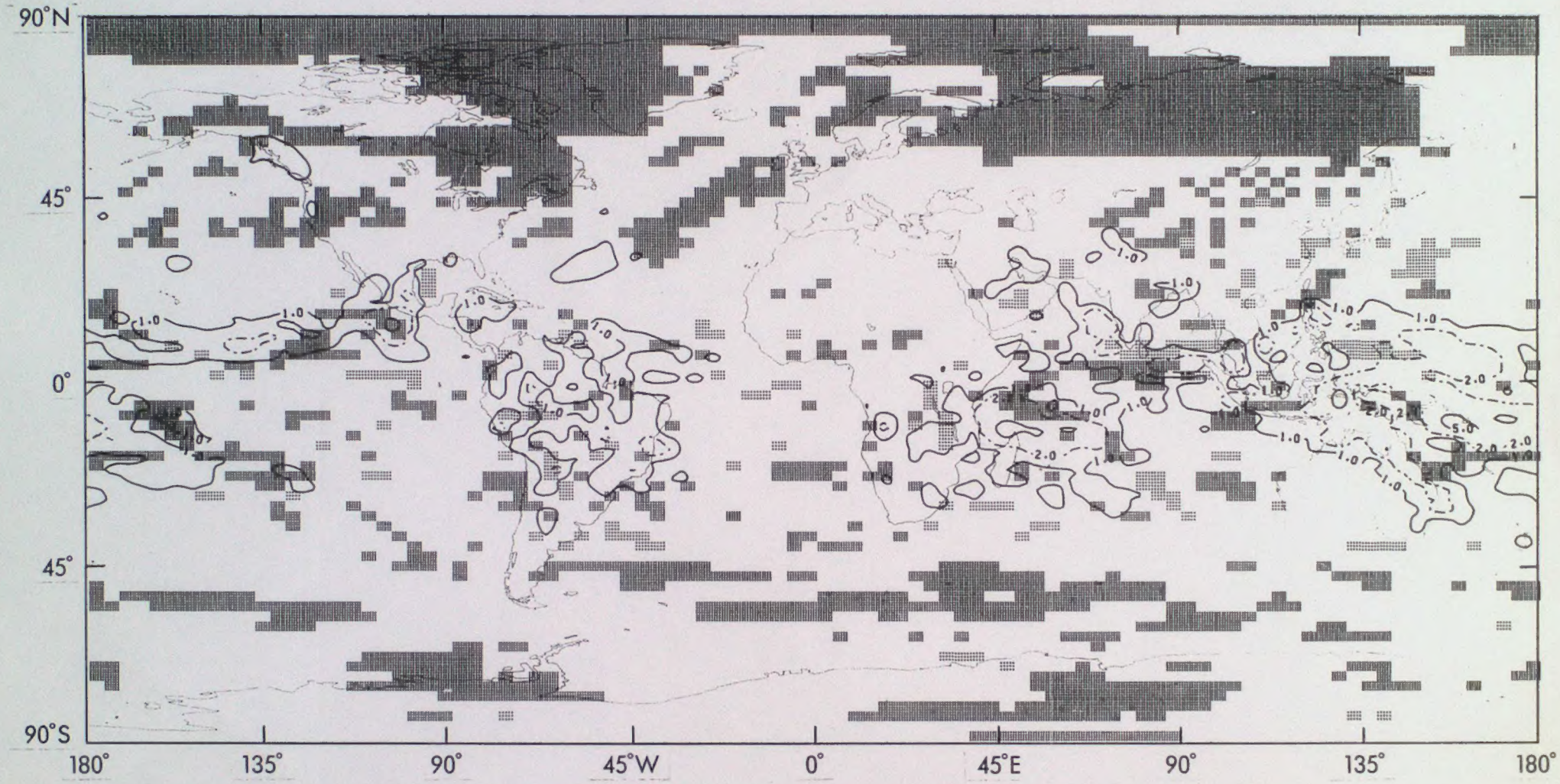

Figure 13b